IN-SITU AND EX-SITU PULSED LASER MELTING AND RAPID LATERAL SOLIDIFICATION OF Al THIN FILMS

by

Hasan Kotan

BS, Sakarya University, 2006

Submitted to the Graduate Faculty of

Swanson School of Engineering in partial fulfillment

of the requirements for the degree of

Master of Science

University of Pittsburgh

2010

UNIVERSITY OF PITTSBURGH

SWANSON SCHOOL OF ENGINEERING

This thesis was presented

by

Hasan Kotan

It was defended on

April 2, 2010

and approved by

J. Gray, Assistant Professor, Mechanical Engineering and Materials Science Department

I. Nettleship, Associate Professor, Mechanical Engineering and Materials Science Department

Thesis Advisor: J. M. K. Wiezorek, Associate Professor, Mechanical Engineering and Materials Science Department

IN-SITU AND EX-SITU PULSED LASER MELTING AND RAPID LATERAL SOLIDIFICATION OF Al THIN FILMS

Hasan Kotan, MS

University of Pittsburgh, 2010

Under extreme conditions (e.g. changes in temperatures and pressures) phase transformations can proceed along various different transformation routes that are not accessible under equilibrium conditions, involving non-equilibrium processes, and can therefore result in various unusual and novel microstructures. The investigation of the transformation path for specific thermodynamic and kinetic conditions and understanding of the resulting microstructural evolution is both scientifically intriguing and technologically important, as many materials properties are strongly dependent on the scale and morphology of the microstructure of a material. Pulsed-laser-irradiation of thin films is a relatively novel processing route that induces melting and rapid re-solidification under extreme conditions of rapid heating-cooling cycles in thin films on amorphous substrates. To date most studies on laser processing of thin films have focused on rapid solidification of Si and Cu thin films.

This thesis reports on the application of pulsed-laser processing and rapid solidification of technologically important Al thin films. It is demonstrated that pulsed-laser melting and rapid re-solidification is feasible for Al thin films in various configurations. Rapid solidification after pulsed-laser melting has been accomplished for Al films on bulk Si supported amorphous

underlayers, with and without a thin synthetic amorphous capping layer, and also on free-standing and electron-transparent (no bulk Si support) Al films on thin amorphous underlayers, with and without thin synthetic amorphous capping layers. This dissertation reports only on a comparison of the microstructures resulting after laser processing of free-standing and electron-transparent (no bulk Si support) Al films on thin amorphous underlayer without thin synthetic amorphous capping layers. Excimer-laser-induced melting and rapid solidification of such Al thin films have been carried out in air. The resulting microstructure has been investigated post-mortem using transmission electron microscopy (TEM). The thin film microstructure resulting from re-solidification after pulsed-laser melting consisted predominantly of directionally solidified columnar grains, approximately 80nm thick (full film thickness), 0.5μm wide and up to 5μm long. Additionally, laser induced melting and re-solidification experiments were carried out using the dynamic transmission electron microscope (DTEM) at Lawrence Livermore National Laboratory, which enabled in-situ observations of the transient phenomena associated with the liquid-solid transformation with its unprecedented 15ns temporal and nano-meter (nm) spatial resolution. The in-situ DTEM experiments were used to study details of the morphology and dynamics at the liquid-solid interface, revealing a planar liquid-solid interface that moves at an average velocity of ~ 3m/s. Ex-situ post-mortem TEM investigations of samples that were laser-processed during the in-situ DTEM experiments showed that microstructures were similar in morphology for the in-situ and the ex-situ rapid solidification experiments.

TABLE OF CONTENTS

LIST OF TABLES

LIST OF FIGURES

PREFACE

This work would not have been possible without the assistance of a number of individuals. First, and foremost I would to thank my advisor Prof. Wiezorek for his guidance and advice throughout my project.

I also want to thank members of the Materials Science and Engineering department, particularly my committee members, Profs. Gray and Nettleship. I also want to thank Dr. Kulovits for his technical assistance, patience and knowledge and the graduate student who I have worked with, particularly, Xiahan Sang and Rong Zhong. Their assistance with experiments and the many discussions I have had with them were invaluable.

Finally I would like to thank my family for the constant support and encouragement. I am thankful for everything they have done for me.

1.0 INTRODUCTION

In the field of materials science and engineering, phase transformations, including solidification from the liquid state, have been important topics of major research activities and have motivated many scientists for years. The properties of the solidified materials are closely related to their microstructures. Hence, one can manipulate the resulting microstructures by controlling the phase transformation pathway during the processing of engineered materials and obtain desired properties. In particular, phase transformations under conditions far-from equilibrium have provided researchers with ample opportunities to obtain unique materials with improved property combinations. For example, rapid solidification techniques, which produce the solid from the liquid under non-equilibrium conditions, have grown in importance because of their ability to generate a variety of nonequilibrium microstructures [1-9, 13-17, 19, 21]. A more recent development has been the utilization of pulsed-laser processing to develop on-equilibrium microstructures in thin films, including for rapid heating, melting and re-solidification [1-8].

The microstructure of as-deposited thin films is often further manipulated via grain growth through either thermal annealing at equilibrium conditions or by application of laser processing at nonequilibrium conditions. The development of the pulsed-laser-based processing of thin films has been widely utilized in studying the details of phase transformations at nonequilibrium conditions because rapid melting of the films and rapid quenching of the liquids

can take place in well-controlled conditions. While the details of phase transformation mechanisms involved in pulsed-laser melting and solidification of some metallic thin films [1-4] and semiconductors thin films [5-8] have been extensively investigated experimentally, such details involving aluminum thin film is very limited. This is somewhat surprising since scientifically rapid melting and solidification of Al thin films and its alloys may result in various phase transformation paths, and technologically aluminum thin films may be utilized in large area electronics, such as interconnection in microdevices in order to deal with problems related to electromigration failure [50, 24].

In this work, we investigate the basic transformation processes that are manifested in re-solidification of Al films after melting by pulsed laser irradiation. We have applied the pulsed laser for melting in air (ex-situ experiments) and also in the high vacuum environment of a transmission electron microscope (TEM). The later experiments conducted in a modified TEM instrument enabled direct observation of dynamic processes during the rapid solidification process (in-situ experiments). We explore the pulsed-laser-induced phase transformation of Al thin films on thin amorphous substrates, which include grain growth from unmelted grains at the sides of the finite scale melt-pool toward the superheated liquids in well-controlled ways resulting in long elongated grains. We also investigate the dynamics of the solid-liquid interface during rapid growth in terms of growth velocity and growth characteristic by using a novel microscope, the so-called dynamic transmission electron microscopy (DTEM). Specifically, Al films have been irradiated by a single pulsed-laser:

(1) In air (ex-situ illumination) to establish the feasibility of rapid lateral solidification of Al films without a synthetic laser-transparent amorphous capping layer, to obtain the critical laser energy values for complete melting of the Al films, and to enable comparison with the dynamic in-situ experiments, which require an electron-transparent film;

and

(2) In the dynamic transmission electron microscope (DTEM) (in-situ illumination) to provide a first systematic investigation of the details of solid-liquid transformation regarding interfacial velocity and growth characteristics. The results of this work, when taken together with what has been obtained previously with other metallic thin films, enable us to develop a more generalized understanding of pulsed-laser melting and resolidification of metallic thin films.

In this thesis, we build an understanding of pulsed-laser-induced melting and resolidification of as-deposited Al films, which may lead to a number of novel and alternative techniques for improving the properties of Al films. The section "Introduction" states the problem and gives general ideas about the study we have performed. The section "Background" provides overviews of basics of conventional solidification as well as rapid solidification of pure metals, driving forces of solid-liquid interface growth characteristics, and several methods to manipulate the microstructure of thin films. Also, experimental methods associated with the deposition of the films, ex-situ illumination system and in-situ illumination system that have been used in this study are addressed. The section "Experimental procedures" provide a brief

review of how the experiments were executed. The section “Problem statement” addresses the problem studied here and states the goal of this study. The section “Experimental results” presents the results of microstructural analyses of as-prepared film, ex-situ and in-situ irradiated Al films and describes the details of phase transformation scenarios and grain morphologies encountered in the pulsed-laser-induced melting and resolidification process of Al thin films. The section “Discussion” provides the current understanding of the experimental results and a comparison of results with other pulsed-laser irradiated metallic thin films. The section “Summary and Conclusions” reviews the results presented in this thesis and suggests possible the future works necessary to improve the understanding of currently inconclusive or indeterminate evidence regarding some of the aspects of the results presented in this thesis.

The objectives of this thesis are to

(1) demonstrate that it is possible to perform pulsed laser melting of electron transparent (less than about 150nm thick) thin films of Al on very thin (50 to 100nm) amorphous substrates with and without thin (50nm or less) capping layers;

(2) reveal details of phase transformations involved in pulsed-laser-induced melting and following rapid lateral resolidification of Al thin films regarding the evolving grain morphology, scale and orientations;

and

(3) determine the solid-liquid interfacial velocity and possible morphological changes of the transformation interface during growth by direct observations in the DTEM.

2.0 BACKGROUND

2.1 SOLIDIFICATION

2.1.1 Basics of Solidification of Pure Metals

The mechanism of crystallization of a liquid is a longstanding classic problem that has attracted the interests of many experimentalists and theoreticians [9]. Most engineered materials of use in daily human life are solidified from the liquid state and the resulting microstructures as well as materials properties are very much dependent on details of this phenomenon. Solidification is, therefore, one of the most important phase transformations in industrial production routes of engineering materials.

Solidification is a classical example of a nucleation and growth processes. Phase transformations in solidification are facilitated by thermal fluctuations and can only occur when probability of transfer of atoms from the parent phase to the product phase is higher than that for the opposite process. However, before this stage of growth of the thermodynamically more stable phase is reached, it is necessary that some volume of this new phase, to which atoms of the parent phase can jump, should already exist. Therefore, stable regions of the new phase, nuclei, have to form by a process called nucleation.

Nucleation is a process in which a new phase appears within the unstable or metastable parent phase by overcoming the kinetic barrier. This kinetic barrier is determined by the sum of the increase of interfacial free energy associated with the interface between the nucleus and the parent phase, which is proportional to the area of solid/liquid interface, and the decrease of the volumetric free energy of the cluster or nucleus, associated with the appearance of the stable phase in the unstable phase [10]. The transition from a highly disordered liquid phase to an ordered crystalline solid phase is accompanied by a lowering in the Gibbs free energy of the material. Figure 1 schematically shows how the free energy changes with respect to the nucleus radius, r. Nucleation is only stable if further growth reduces the energy of the system (Fig. 1).

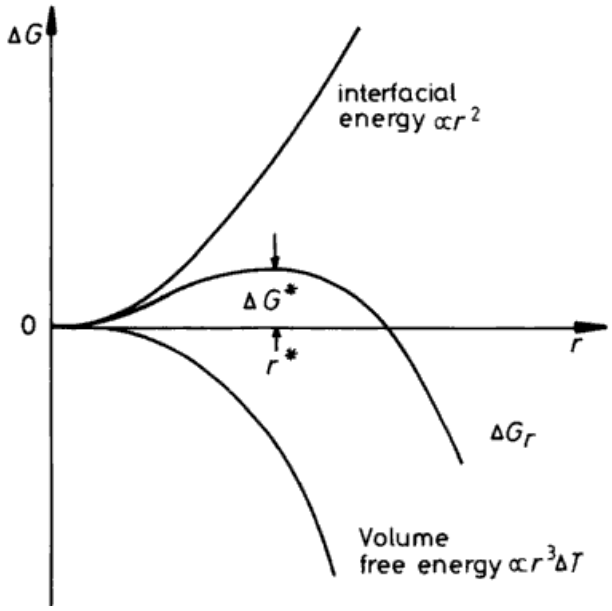

Figure 1. Critical radius for nucleation [10]

Nucleation begins at some degree of undercooling. In metals undercooling is generally very small and increasing the undercooling has the effect of markedly increasing the nucleation rate as well as the growth rate of the new solid. The details of nucleation dominate the processes at the beginning of solidification and have important effects on the resulting microstructure of the crystal [11].

Once nucleation has occurred, atom transfer from the thermodynamically less stable liquid to the crystals has to continue in order to ensure their growth. This is called crystal (grain) growth and is defined as the increase of nuclei in size by addition of atoms from the liquid phase. During growth the solid-liquid interface is an active free boundary from which latent heat is liberated during phase transformation. This heat is conducted away from interface through the solid and liquid, resulting in the presence of thermal boundary layers near the interface. The flow direction of the latent heat released at the interface is determined by the magnitude of the temperature gradient on both sides of the liquid-solid interface and strongly affects final microstructures. The density changes across the solid-liquid interface. If the density of solid is greater than that of liquid the material shrinks upon solidification [12].

During the first stage of solidification, which is essentially nucleation-controlled, the volume fraction of the solid is still very small. After some time, the temperature of the system has risen above the nucleation temperature and the second stage of solidification becomes growth-controlled. In this stage, the number of grains present thus remains essentially constant and the growing crystals steadily consume the melt and eventually impinge upon each other to form a structure of grains.

2.1.2 Rapid Solidification

The differences between conventional solidification and rapid solidification lie in the extreme cooling rates. Under near equilibrium conditions such as conventional casting there is a solidification pathway from the liquid to the stable solid state and the system is cooled down slowly with cooling rates ranging between 10^{-3} and 10^{3} K/s [13]. On the other hand, under extremely high cooling rates, as such, the physics of rapid solidification deviates from that of a normal solidification process and non-equilibrium phases can form as a result of being favored kinetically over equilibrium phases. This can result in constitutional changes and in difference in the morphology and scale of microstructures [14, 15].

It is well known that the spectrum of materials with different properties is greatly enhanced by rapid quenching of the liquid [13]. Modern manufacturing industry uses increasingly sophisticated processing methods in order to produce complex materials and microstructures to meet stringent component performance targets. Rapid solidification processing provides many examples of these manufacturing methods and expanded the range of possible technologically relevant applications for different materials, metals and alloys [16, 15]. In most industrially relevant cases of rapid solidification processing, the large melt undercooling produces very high rates of solidification that inherently involve nonequilibrium kinetics of phase change and coupled transport of energy and species. This coupling ultimately determines the phase selection, microstructure formation and final properties of the rapidly solidified materials [17].

The expression Rapid Solidification Technology (RST) is used to refer to a large number of techniques and processes used in laboratories and industries to quench metallic metals and alloys from the melt at cooling rates exceeding 10^3 K/s. Melt spinning, laser or electron beam surface resolidification, and spray deposition have demonstrated very successfully that extremely high cooling rates can be obtained by such techniques [16]. All of these techniques may be thought of as casting where at least one physical dimension is small so that heat is extracted more rapidly than in conventional casting.

Rapid solidification is applied to materials to improve their properties and facilitates (1) substantial extension of solid solute concentrations beyond the equilibrium concentration limits in alloys, (2) extreme refinement to the small scale or grain sizes or fabrication of extremely large grain size in the solidified metals and alloys, (3) formation of new metastable crystalline phases, (4) formation of the so-called metallic glasses [18, 19].

2.1.3 Solidification Interface

From a thermodynamic point of view, solidification requires heat flux from the system to the surroundings, which changes the free energies and therefore the relative thermodynamic stability of the phases involved [20]. In pure metals, solidification is controlled by the rate at which the latent heat of solidification can be conducted away from the solid-liquid interface. Conduction can take place either through the solid or the liquid depending on the temperature gradients at the interface. For example, a negative temperature gradient at the liquid side of the liquid-solid interface indicates that the latent heat will be dissipated almost exclusively into the undercooled

melt. A positive temperature gradient, however, ensures that the latent heat is removed through the solid and very little, if any, through the liquid [21].

In the pure substance the stability of solid-liquid interface depends on the direction of heat flow. When a solid grows into a super heated liquid (positive temperature gradient in the liquid) a planar solid-liquid interface is stable (Figure 2 (a)). Local fluctuations in the interface velocity can create protrusions of solid into the liquid, a perturbation in the planar solidification front forms. If the solid grows into the superheated liquid such a perturbation is not stable. The temperature gradient in the liquid will increase while the gradient in the solid decreases. Since the heat flux is proportional to the temperature gradient, more heat flows into the solid at the tip of the perturbation, which cannot be transported away resulting in a decrease of the local growth rate below that of the planar regions and the perturbation will disappear. On the other hand, when a solid grows into a supercooled melt (negative temperature gradient in the liquid) a planar solid-liquid interface is not stable (Figure 2 (b)). If a thermal fluctuation induced perturbation forms at the interface the negative temperature gradient in the liquid becomes more negative and permits the tip to reject more heat. As a result, the local growth rate is increased for the perturbation relative to the planar interface sections and the interface becomes always morphologically unstable [22]. Figure 2 shows heat flow in a solidifying system with respect to temperature distribution.

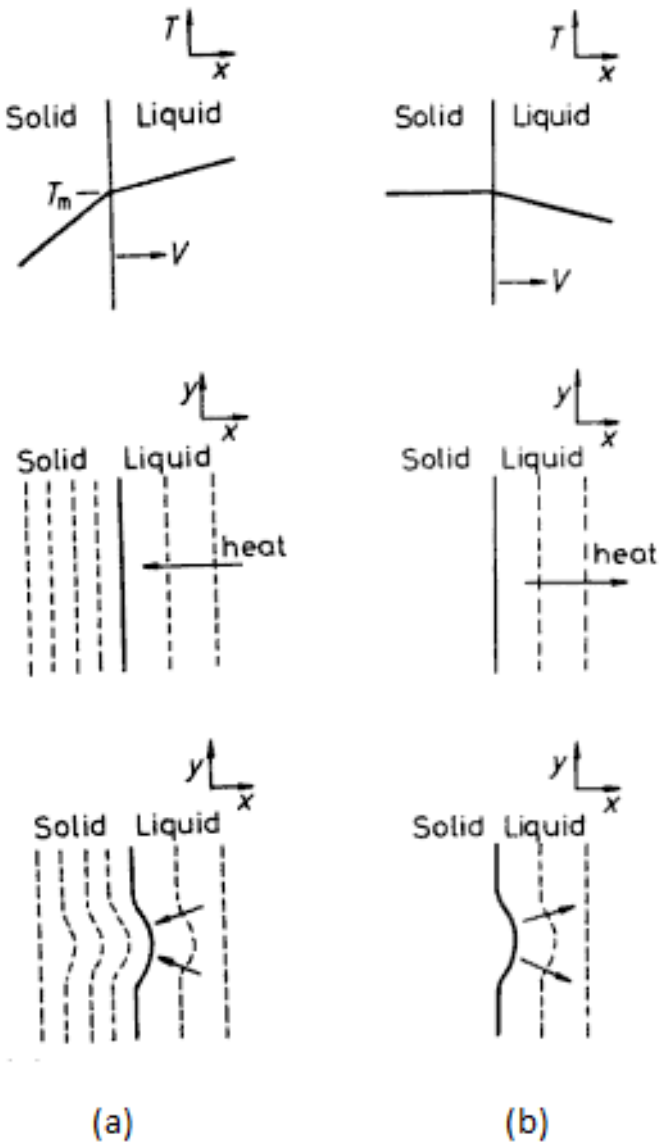

Figure 2. Temperature distributions for solidification when heat is extracted through (a) the solid, (b) the liquid [10]

2.2 PULSED-LASER PROCESSING OF THIN FILMS

Microstructure evolution and control in thin films are of current technical interest for obtaining high-performance thin film transistors (TFT) [5] for advanced applications. In order to improve device performance and uniformity in advanced applications, control of grain size and grain location are required. Pulsed-laser processing technique offers the ability to manipulate grain structures and microstructure at precise locations under controlled solidification conditions [2] and have been used to modify thin films for advanced applications. The purpose of the process is to manipulate the grain size and grain-boundary-location or arrangements by controlling the grain growth. Figure 3 shows an example of modified grain microstructure of a Si thin film used in device applications.

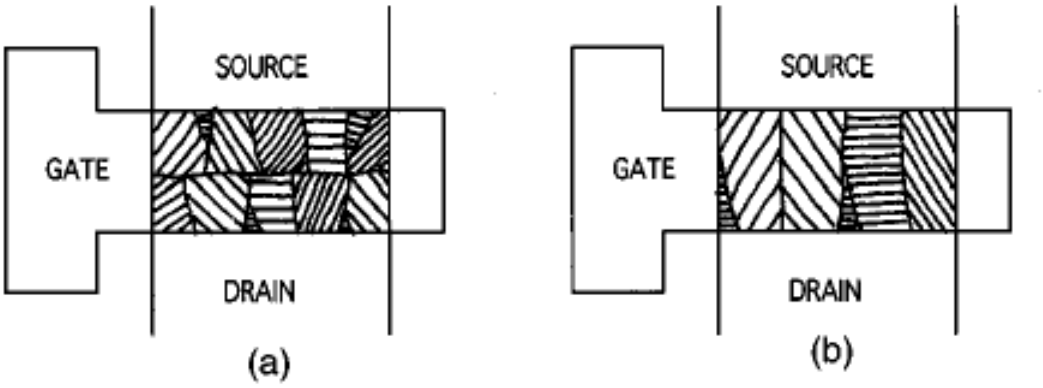

Figure 3. Schematic view of strategically placed TFT device on grain boundary location controlled Si films such that (a) a single perpendicular grain boundary and (b) zero perpendicular grain boundaries are encountered by the traveling majority active-channels regions [23]

Laser treatment of a thin film involves directing a high power beam of laser irradiation onto the surface. A certain fraction of the laser is absorbed at the surface by excitation of the electronic system of the solid and subsequently converted to heat by carrier scattering and

phonon formation. Large amounts of the energy are deposited into small volumes on time scales which can be exceedingly short; thus the system is rapidly heated to and then rapidly quenched from a highly excited state, allowing the observation of transient phenomena and metastable states not previously seen [24, 36]. The phase transformation kinetics of laser-induced melting of solid films is mainly determined by laser absorption, heat conduction through the substrate or the film, and energy consumption associated with melting of the material. The heat transfer is important for modifying the microstructure and is a function of heat capacity, absorption coefficient, thermal conductivity of materials, and heat of transformation [1-2, 37]. Therefore, solidification characteristics may be entirely different depending on the process parameters.

2.3 THEORETICAL FINDINGS ON PULSED LASER PROCESSING OF THIN FILMS

Many researchers have conducted significant investigations on the phase transformation kinetics involved in pulsed-laser induced melting and solidification because it allows rapidly heating and solidifying of thin films. Pulsed-laser processing and following rapid solidification has numerous advantages in modification thin film structures such as: (1) independently adjustable parameters, including the laser heat fluence, film thickness, substrate thermal conductivity, and substrate temperature, to allow controlled melting and solidification over wide range of thermal conditions, and (2) large-area large-grain microstructures in uniformly thick films can be produced which are amenable to detailed quantitative and statistical analysis of the crystallographic orientations, textures, grain boundaries, and defect network [1]. Pulsed-laser induced melting has been applied successfully to semiconductor and metallic thin films under different names.

2.3.1 Controlled-Super Lateral Growth (C-SLG) of Si Films

Controlled-super lateral growth (C-SLG) process is a pulsed-laser processing technique and enables formation of large poly-crystals from amorphous Si films as a consequence of the liquid phase regrowth from the discontinuous and small solid seeds, which are never fully melted under irradiation. Grains can grow from the partially melted regions adjacent to the completely melted regions, resulting in a microstructure containing large grains with uniform length and well-controlled grain-boundary-location [6].

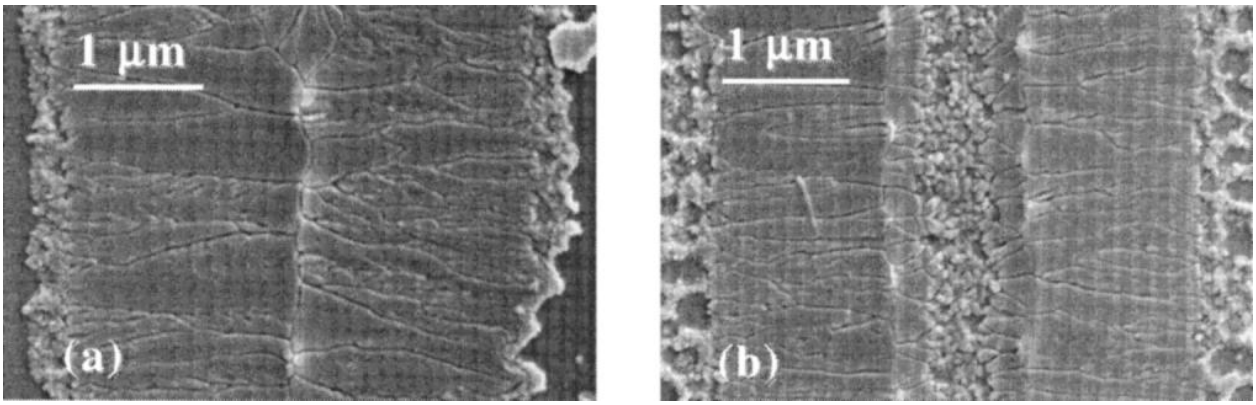

Figure 4. SEM micrographs of a Si sample (100 nm thick), irradiated by the short pulse at RT and different energy densities (a) elongated grains, (b) elongated grains have been ruined by nucleation at the center-line location of the melted trench [25]

Figure 4 shows SEM micrographs of irradiated Si grains. There is a limit (~ 1.5 µm) to the maximum lateral growth distance as continuous cooling of the liquid layer via conduction to the substrate eventually lead to nucleation of solids at the interface between the supporting bulk material and the super-cooled liquid ahead of the laterally growing solidification interface and any further lateral growth is prevented.

Growth distances could be extended if the width of the completely melted region is made sufficiently narrow so as to avoid the nucleation of solids in the supercooled liquid, the advancing C-SLG grains originating from the two unmelted sides eventually impinge on each other and form a well-defined grain boundary at the center of the molten region. Another way to overcome the nucleation problem is elevated substrate temperatures. Increasing the substrate temperatures leads to decreased quenching rates, which in turn provides more time for lateral growth to take place before bulk nucleation intervenes to terminate lateral growth [25].

2.3.2 Sequential Lateral Growth of Si Films

Although the controlled super-lateral growth (C-SLG) processing technique enables manipulation of microstructure of Si films in predictable ways, the maximum lateral growth distance is limited to a few micrometers due to the nucleation process in the supercooled liquid in front of the advancing interface of SLG grains. A new method, termed sequential lateral solidification (SLS), has been developed to overcome this weakness of C-SLG. Development of the sequential lateral solidification (SLS) process is based on multiple sequential irradiations by using a straight mask. In the SLS technique, the sample is translated in one direction, leading to a microstructure with parallel grain boundaries along the translation direction. The advantage of the SLS process is related to the flexibility in mask designs, which facilitates preparation of grain-boundary-location controlled materials with various shapes and sizes of grains, and can lead to single crystal materials in the processed regions [5, 25].

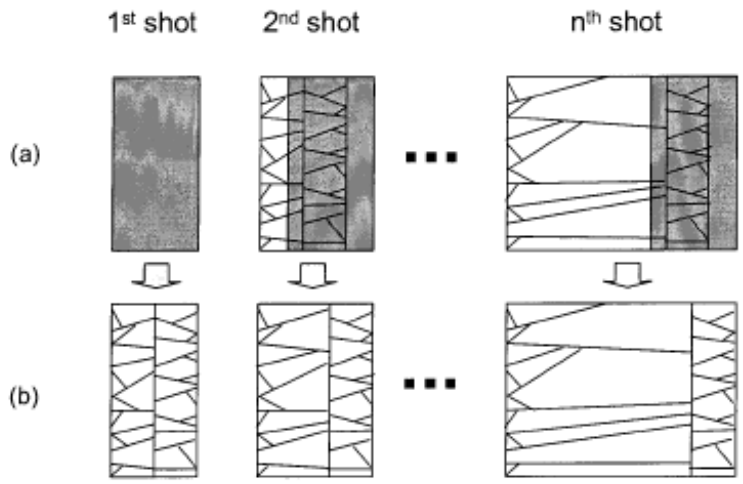

Figure 5. Schematics of sequential lateral solidification (SLS) process: (a) laser irradiation and (b) resulting microstructure [24]

Figure 5 shows a simple schematic diagram illustrating the SLS process. In particular, the grains formed during the first pass can act as seeds, allowing the regrowth in the amorphous region, which is completely melted during the second pass.

2.3.3 Rapid Lateral Solidification of Metallic Thin Films

Pulsed-laser irradiation is currently being used to modify pure metal thin films deposited on silicon wafer substrates [1-4]. In the process, a pulsed excimer laser is used to completely melt selected regions of a polycrystalline metallic thin film. After melting, rapid conduction of heat into the substrate results in quenching and supercooling of the molten pool. Unmelted grains at the sides of the pool initiate lateral solidification toward the center when the local temperature reaches the melting point, resulting in long elongated grains growing into a cooling liquid melt. Figure 6 shows a schematic of pulsed laser induced melting a RLS for Cu thin films on amorphous substrate.

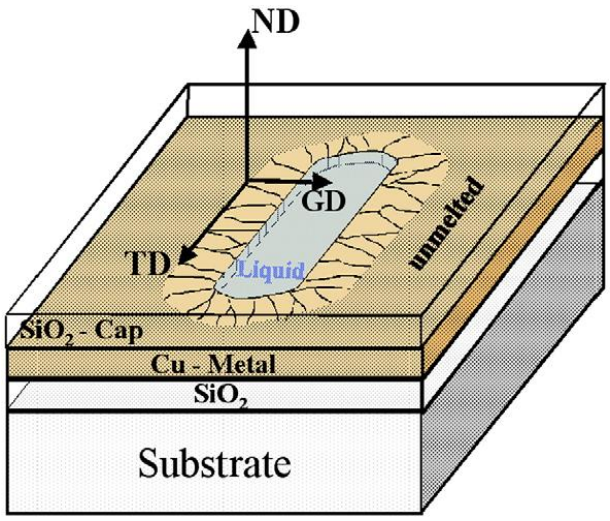

Figure 6. Schematic of geometrically confined Cu thin film on Si substrate with a single pulsed laser melted and partially solidified Cu line. ND; film normal direction, TD; the transverse direction, GD; in plan growth direction [3]

Compared to the explosive crystallization, which provides little opportunity to manipulate the microstructure of the thin films, the various melting and solidification pathways encountered in the pulsed-laser processes in metallic thin films can lead to diverse microstructures. In particular, researchers at University of Pittsburgh have presented microstructure modification scenarios of Cu thin films based on grain size variation and revealed that rapid lateral solidification (RLS) of Cu thin films of 150 nm thickness via pulsed-laser irradiation enables preparation of elongated grains up to 22 μm in length [2]. Prior work on Cu thin film RLS also established that after resolidification four morphologically distinct zones result in the pulsed laser illuminated region [2]. These distinct zones have been termed (1) occlusion zone, in which the width of some grains increases at the expense of others and grains quickly expand vertically in the beginning of solidification; (2) columnar growth zone, in which grains surviving from the occlusion zone now grow laterally up to 17.5 μm; (3) defective growth

zone, in which elongated grains break down during the final stage of lateral growth; (4) nucleation zone, where nucleation at the interface of the liquid metal with the substrate in the undercooled melt occurs. The heat flow in the irradiation geometry used to modify Cu thin films with bulk substrates [e.g. 2] is predominantly vertical into the substrate, resulting in critical supercooling required for nucleation during the final stage of resolidification. Lateral growth ceases by encountering the nucleation of new grains in the nucleation zone during RLS of Cu thin films [2].

It is known that metallic films de-wet upon annealing in the solid as well as in the liquid state [38] since thin films of molten metal on amorphous substrate are unstable with respect to de-wetting and the Gibbs free energy of the system is lowered by liquid agglomeration that leads to uncovering of the solid substrate. Therefore, control of de-wetting in thin liquid films is a significant technological problem. It has been proved in prior research [4] that the typical liquid phase de-wetting process can be suppressed with the use of an additional capping layer of SiO_2 on the thin metal film, essentially encapsulating it between substrate/underlayer and the capping layer (e.g. Fig. 6).

2.4 EXPERIMENTAL METHODS

2.4.1 Sputtering Deposition

The deposition processes for metal thin films typically include evaporation or sputtering or chemical vapor deposition. In this work, a magnetron sputter deposition system has been used for deposition of Al thin films on amorphous substrate at room temperature. In contrast to other techniques, sputtering typically removes two to five atoms from the surface of the target per incident ion and thus limits the total change in concentration or composition for alloy deposition [26]. In addition, amorphous cap-layers such as SiO_2 might be necessary for the thin film system and in case of deposition with e-beam evaporation, for example, high melting temperature could be a critical problem for the system. Sputtering deposition technology overcomes all these problems and enables preparation of amorphous, laser-transparent oxide encapsulated metal thin films on appropriate substrates.

Sputtering deposition is a physical vapor deposition (PVD) method of depositing thin films and involves bombardment of a target by ions accelerated in inert gas plasma, such as Ar. The ion-target collision process, typically involving energies of hundreds of eV, results in the ejection of atoms from the target materials, which then deposit onto a substrate. The sputtered species can be neutral atoms or ionized atoms or ionized atom clusters (ions), and their interaction with the plasma involves complex interactions and energy exchange. A wide variety of sputtering techniques including direct current (DC) and radio frequency (RF) discharge, magnetron, and ion beam sputtering have been developed [26, 27] for different purposes.

Larger grains in the initial microstructure of as-deposited film are preferable in pulsed-laser irradiation. Various microstructures of the as-deposited films can be obtained by changing the deposition parameters, including deposition temperatures, in a sputtering system. Figure 7 shows schematically the microstructural evolution in thin metal films as a function of normalized temperature and sputtering pressure.

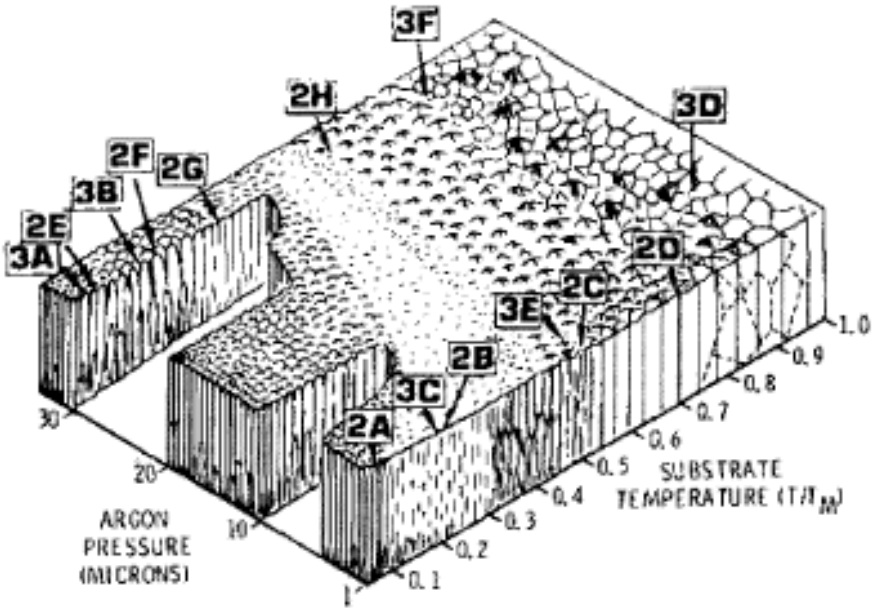

Figure 7. Schematic representation of deposited microstructure with respect to the normalized substrate temperature and sputtering pressure [28]

This diagram shows that the microstructure of as-deposited polycrystalline metal films depends on the deposition temperature. Specifically, as-deposited films have larger grains when they are deposited at elevated temperatures due to higher mobility of the add-atoms on the substrates. As well as the large grain size, the improved step coverage of the metallic thin films deposited at high temperatures have encouraged many researchers to use a high-temperatures sputtering deposition process to obtain required thin films [28].

2.4.2 Excimer Laser Illumination System

An excimer laser illumination system is used to modify the microstructure and properties of thin films after deposition, while avoiding the difficulties of conventional heat treatment [1]. This process has significant advantages in manipulating the microstructure of the film over the conventional process including the flexibility in mask design which makes possible grain-boundary-location controlled films with various shapes and sizes of grains. It is used to melt thin films of virtually any composition, which can rapidly resolidify under a wide range of conditions and is capable of producing unique properties not otherwise available.

The projection illumination system consists of a Lambda Physik EMG-202 KrF excimer laser operating at 248 nm wavelength with 28 ns pulse duration. A collimating telescope, energy meter, a single slit Cu mask, and a single fused silica lens positioned for a 5X demagnification are also other part of the laser used to manipulate the laser beam. Figure 8 shows a schematic view of illumination system.

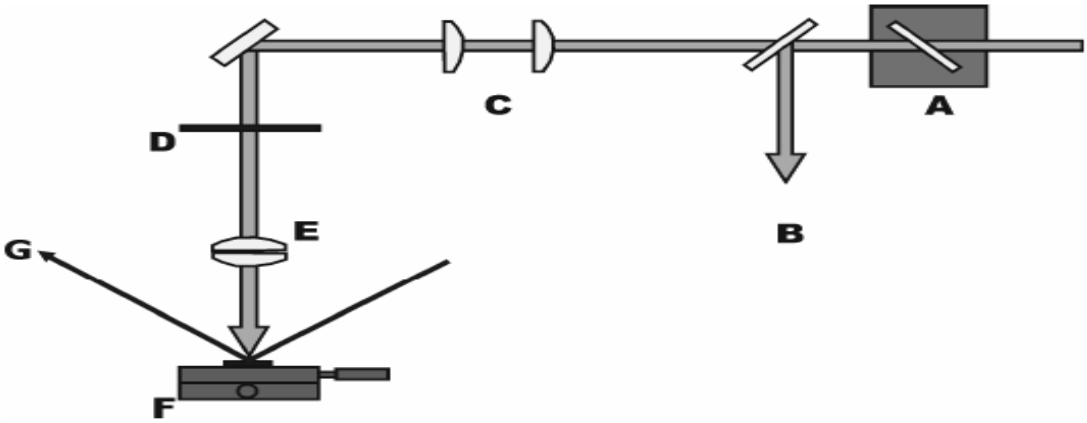

Figure 8. The 5X demagnification illumination system used in the ex-situ pulsed laser melting experiments A) variable attenuator, B) energy meter, C) telescope, D) mask, E) imaging lens, F) translation stage, G) Transient Reflectance system for Si surface melting calibration

Uniformity in the projected line is ensured by irradiating a 50 nm a-Si film on SiO_2, which undergoes striking color changes at known fluence thresholds for surface melting and full melting, respectively [4]. After calibration, the critical incident energy density required for complete melting of a continuous film is determined experimentally. The samples are irradiated at various energy densities to find out the critical energy. For low fluences, for example, the film layer is heated to temperatures not exceeding the surface threshold of the film. For slightly higher fluences, the surface of the film is heated above the melting point, but the melt depth does not penetrate the full depth of the film which resulted in partial melting and partial melting causes vertical solidification that destroys lateral growth. Finally, fluences substantially higher than the partial melting threshold result in complete melting of the thin films [29].

2.4.3 Dynamic Transmission Electron Microscopy (DTEM)

During the last years the possible application fields of pulsed laser irradiation exhibited a continuous increase on material modifications [33]. However, because of the high energy intensity in a very short time and small dimension of the material, melting and resolidification processes becomes very fast causing interface velocity increasing dramatically. It is inherently difficult to experimentally determine the atomic structure of solid-liquid interface in non-transparent media, e.g. in metals [30, 32]. In special cases it might be worth achieving a real time control of the condition of the interface microstructure during the laser modification.

TEM has been used for in-situ experimentation with remarkable success but it has so far not been capable to provide the required time resolution to study the transformation interface in rapid solidification as the interface velocity is too fast. Conventional in-situ TEM experimentation uses TV-rate acquisition via electron compatible camera systems, usually involving charge-coupled devices (CCDs), enabling 1/30 s temporal resolution per single frame. Thus, many important rapid transformation processes in materials science occur on time scales that are currently not accessible to conventional TEM microscopes [31]. Achieving higher time resolution requires a new approach, which is accomplished in a unique instrument, the dynamic transmission electron microscope or DTEM [32-33]. The most current DTEM is based on a modified JEOL 2000FX 200kV TEM with nanosecond time resolution [34-35]. A schematic representation of dynamic transmission electron microscope is shown in Figure 9.

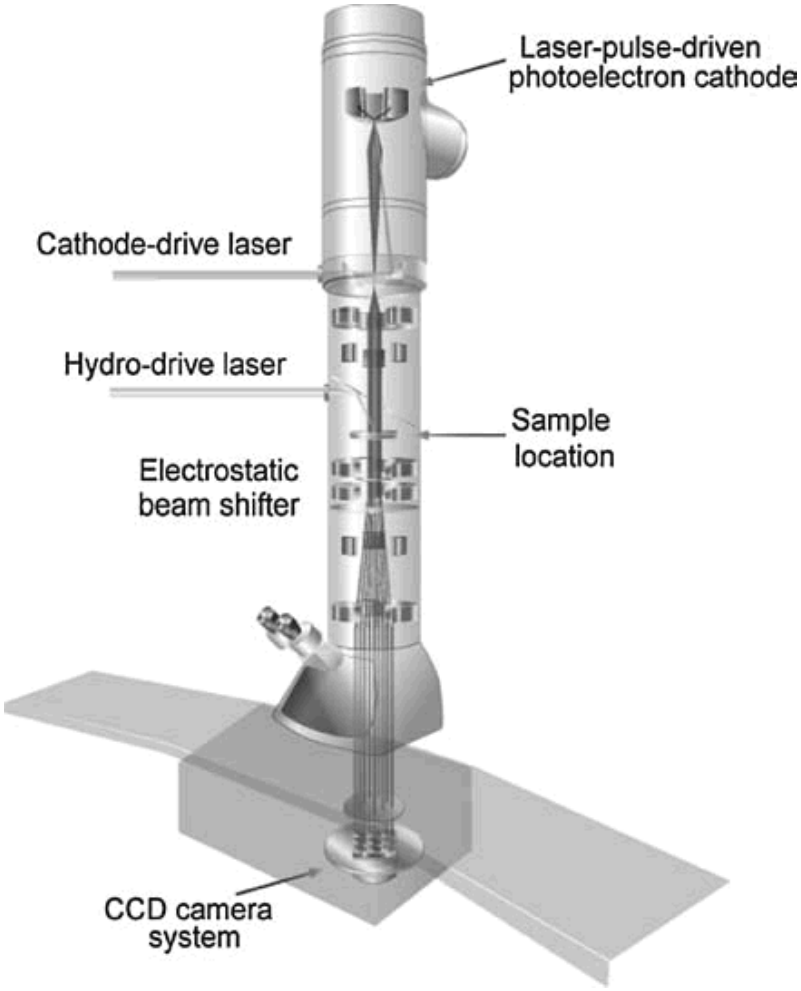

Figure 9. Schematic illustration of a DTEM [34]

The DTEM instrument does not facilitate continuous observations. It is a single-shot pump-probe type of instrument as described in the following. To obtain a DTEM micrograph image or diffraction pattern, a short, intense laser pulse from the hydro-drive laser is used to, locally, at the site of interest, heat the specimen and induce a transformation. This is the pump-pulse. A synchronized laser pulse from the cathode drive laser is emitted time delayed (as short as 15ns) to irradiate the photoelectron cathode and thereby produces an electron pulse (Figure 9). This is the probe-pulse. The probe-pulse illuminates the specimen at the site of interest allowing

to image and observe the change induced by the transformation after the selected preset time delay of as short as 15 ns. Data can be collected in form of images and diffraction patterns. The temporal resolution of the DTEM is therefore limited to about 12 ns, namely, the nominal duration of a sufficiently bright and sufficiently coherent electron pulse emitted from the electron gun of the instrument.

The unique combination of nanometer spatial and nanosecond temporal resolution of the DTEM makes it possible to monitor and investigate details of transformations and changes in materials that occur within nano-seconds in response to the external stimulation [31-33]. One of the main limitations of the in-situ observation by DTEM is that specimens must be sufficiently thin so that the electron beam can readily pass through for recording of images and/or diffraction patterns.

3.0 PROBLEM STATEMENT

Details of phase transformation mechanisms and the resulting microstructural morphologies associated with the re-solidification of thin metal films of Cu and Ag have been studied in prior and ongoing research. For the case of Al thin films and in free-standing films without a bulk substrate support details of the transformations in response to laser melting remain to be elaborated. Unlike Cu and Ag, the face-centered metal Al has high-stacking fault energy and room temperature (≈300K) represents a significant fraction of its melting point (Tm≈935K). These characteristics are expected to influence the formation and redistribution of crystal defects in the crystal formed by rapid re-solidification after pulsed laser melting and perhaps also affects the details of the dynamics at the liquid-solid growth front during the phase transformation. To date knowledge of details of the transformation from liquid to solid after pulsed laser melting of aluminum thin film is very limited. This is somewhat surprising since scientifically rapid melting and solidification of Al thin films and its alloys may result in various phase transformation paths, and technologically aluminum thin films may be utilized in large area electronics. The goal of this research is to evaluate the phase transformation and the modified grain morphology, scale and orientations of Al thin films in response to intense pulsed-laser irradiations. This evaluation will focus on: (1) the feasibility of the study will be tested by performing ex-situ melting in air and results will be evaluated with respect to modified grain morphology as well as comparison to other modified metallic thin films; and (2) the solid-liquid interface velocity will be measured

and the transformation interface growth characteristics will be determined by using a unique instrument, the dynamic transmission electron microscope (DTEM), which provides nano-scale temporal and nano-scale spatial resolution required here.

4.0 EXPERIMENTAL PROCEDURE

4.1 FILM DEPOSITION AND CHARACTERIZATION

Two sets of 80 nm thick Al film samples with and without 50 nm amorphous silica, a-SiO_2, cap-layer were prepared via magnetron sputter deposition on Si-substrate TEM grids with a 100 nm thick membrane of amorphous silicon nitride, Si_3N_4, and 500 µm by 500 µm square shape electron transparent windows using a base pressure of $5x10^{-6}$ Torr**,** working pressure of 5 mTorr Ar, and 100 W target power. The cap layer was deposited using the same working and base pressure but a different target power of 200 W. The deposition rates for the Al films and the cap layers were 2.3 and 0.21 Å/s, respectively.

A JEOL 2000FX 200kV TEM and a Philips XL 30 FEG-SEM microscope were used to characterize the crystallinity, grain size, and film morphology of the aluminum films. KLA Tencor Alpha-Step IQ surface profiler with up to 0.1 nm or less resolution was used to determine the film thickness.

4.2 EX-SITU PULSED-LASER ILLUMINATION

Ex-situ rapid lateral solidification (RLS) experiments were performed using a pulsed excimer laser with an illumination system as schematically shown in Figure 8. To ensure complete melting, i.e., uniform energy across the illuminated sample area by the projected laser light line the illumination system was calibrated using a 50 nm thick amorphous silicon (a-Si) film on a SiO_2 calibration sample. A single laser pulse with a fluence of 130 mJ/cm^2 was used to completely melt the Al thin films. A schematic view of illumination and following resolidification is shown in Figure 10.

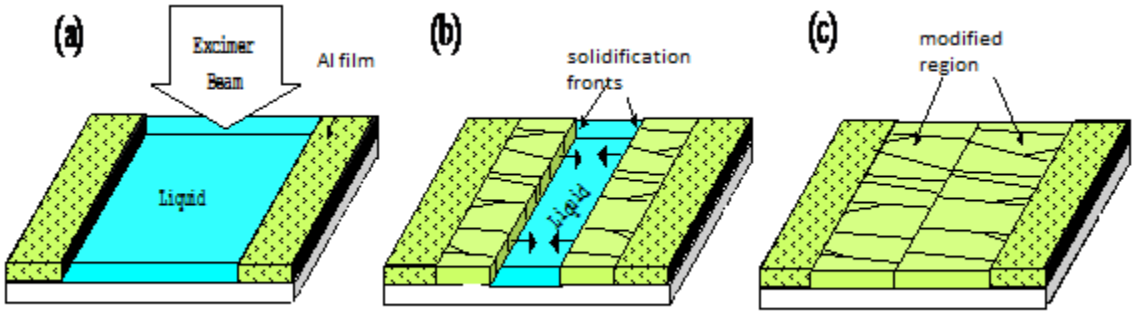

Figure 10. Schematic of Al thin films on Si_3N_4 substrate with a single pulse laser (a) melted, (b) partially solidified, and (c) complete solidified

After the illumination of the sample, a JEOL 2000FX 200kV TEM and a Philips XL 30 FEG-SEM microscope were used to characterize the grain size and film morphology of the modified aluminum films.

4.3 IN-SITU PULSED-LASER ILLUMINATION

In-situ study of the re-solidification after pulsed laser melting has been performed using the DTEM. In these experiments the hydro-drive laser illuminates an elliptical area on the specimen as the laser beam hits the sample at a 45° angle relative to the optic axis of the TEM instrument. Single laser beam pulses with the fluences between 1.5 J/cm² to 3.8 J/cm^2 and pulse duration of 15 ns were used to melt uncapped 80nm thick Al thin film samples on TEM transparent grids. Depending on the laser power used, i.e., the fluence of the single laser pulse, the size of the melted elliptical area ranges from 40-80 µm along the major axis. After illumination, a synchronized laser pulse from the cathode drive laser is emitted time delayed (as short as 15ns) to irradiate the photoelectron cathode and thereby produces an electron pulse. This pulse illuminates the specimen at the site of interest allowing to image and observe the change induced by the transformation after the preset time delay of as short as 15 ns. Data were collected in form of images and diffraction patterns.

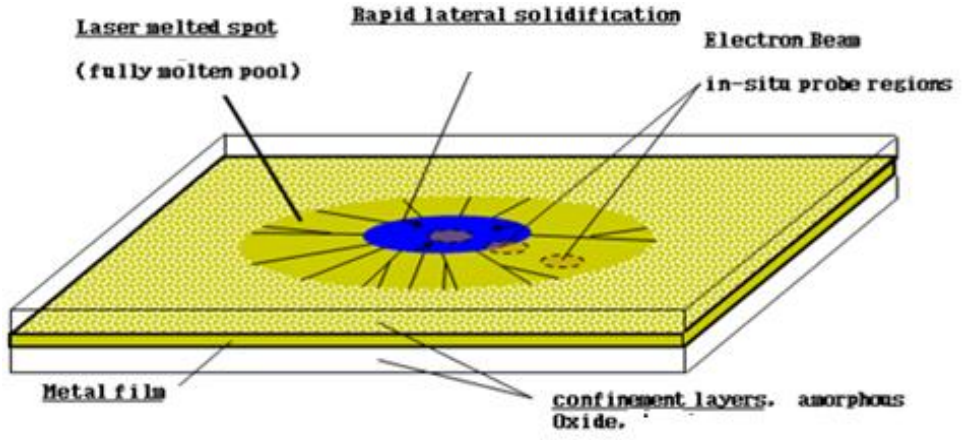

Figure 11. Schematic of line illumination in the experiments. The liquid molten pool is represented as the blue region.

Only a single diffraction pattern or image can be acquired for each pump laser heating pulse. Since the microstructure is modified significantly after one laser shot, a new region was studied for each pump probe experiment and the results are compared. This is applicable since the films used in the study have a uniform thickness and homogeneous microstructures. A series of images taken during several experiments at different time delays allows the characterization of the solid/liquid interface kinetics.

5.0 EXPERIMENTAL RESULTS

5.1 AS-DEPOSITED FILM MICROSTRUCTURE

80 nm thick Al thin films were deposited on electron transparent Si_3N_4 substrates. The thickness was determined with the surface profiler. Transmission electron microscopy (TEM) was used to characterize the crystallinity, grain size, and film morphology of the as-deposited Al thin films.

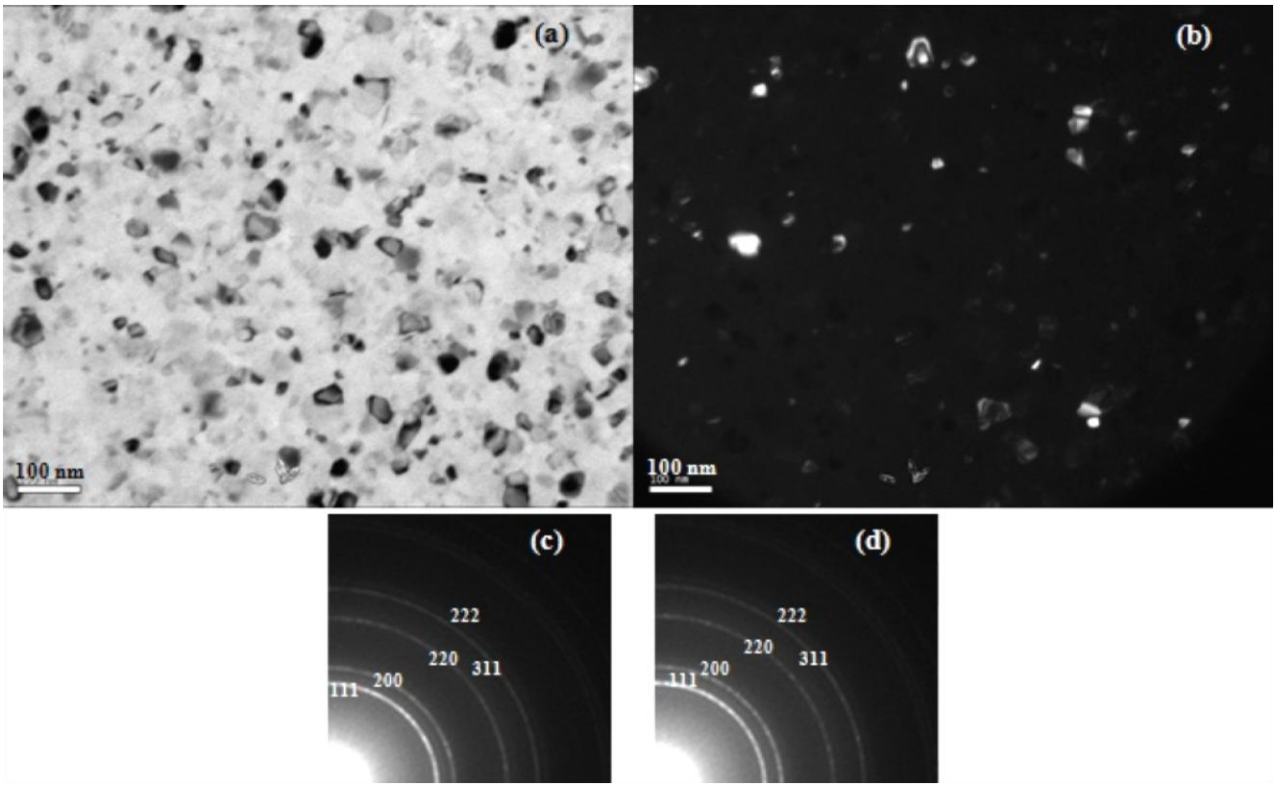

Figure 12. (a) Bright field and (b) Dark field images of the as deposited film, (c) Large area selected area diffraction pattern, (d) Large area selected area diffraction pattern after 30 degree tilt

A bright field (BF) TEM image, a dark field (DF) TEM image and two selected area diffraction patterns (SAD) are shown in Figure 12. The diffraction patterns in Figure 12c and 12d show nearly continuous ring patterns typical for polycrystalline materials with ultra-fine grained or nano-crystalline grain size. 30 degree tilting experiments did not yield discernible changes in the selected area diffraction (SAD) pattern (Figure 12d). Hence, strong fiber texture with respect to film normal is not present in the as-grown Al films. The diffraction rings could be indexed as Al (111), (200), (220), (311), (222) reflections.

Bright field images (e.g. Figure 12a) showed that film microstructure is continuous, which is very important for the rapid solidification experiments, as any possible discontinuity in the initial film affects solidification characteristic. The grains are of equiaxed shape in plan-view. The dark field images as shown in Figure 12b were analyzed with the NIH Image image processing analysis program to determine initial average grain size of the Al thin film prior to the melting experiments. A fixed threshold that would identify features above a certain brightness level as individual grains in the dark field images was implemented. Subsequently the diameter of the 'grains' identified in this manner was measured automatically. The average grain size determined by these analyses was D=17 nm with the deviation of ± 16 nm. The average grain size of 17 nm is a simple geometric average, obtained from measuring over 100 numbers of grains.

5.2 EX-SITU RLS MICROSTRUCTURE

5.2.1 Melting Experiments

In a serious of experiments, 80 nm Al films without caplayer were irradiated with a single rectangular line shaped excimer pulses with adjustable line width. Detailed analyses of the beam intensity profile and the calibration procedure described in section 2.4 were used to determine the fluence in the projected line. After melting and resolidification, the irradiated regions were examined by TEM (e.g. Figure 13 and Figure 14).

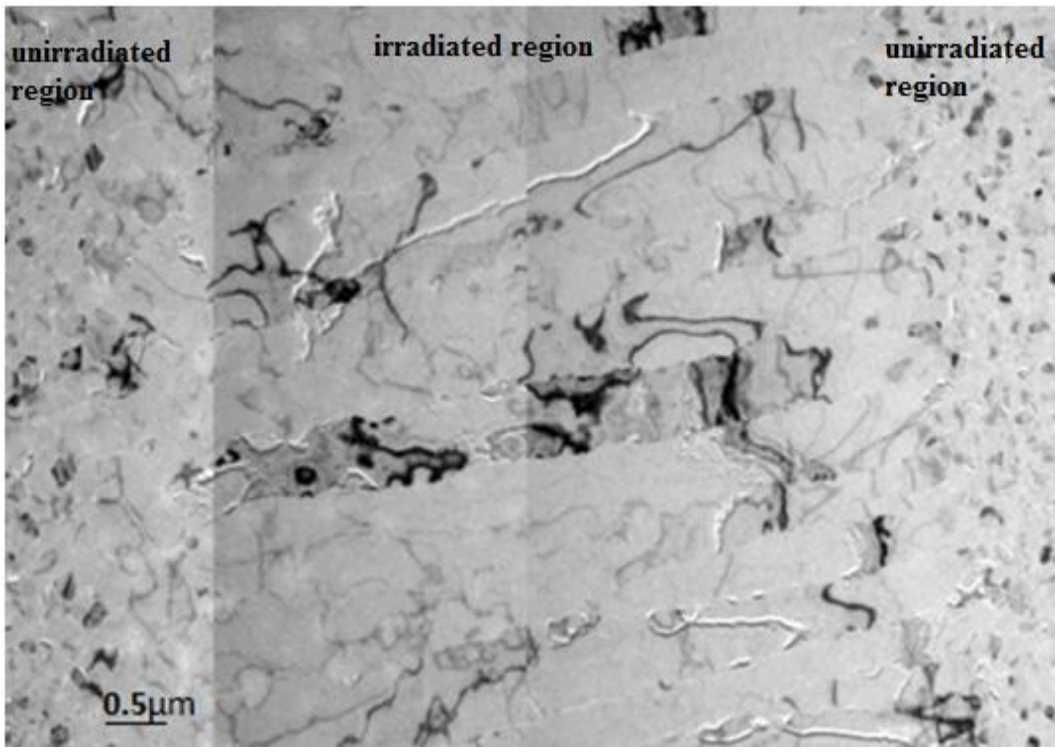

Figure 13. Ex-situ illuminated area and elongated grains

Figure 13 shows a typical TEM image of single-pulse-irradiated uncapped Al film with the laser energy density of 130 mJ/cm² obtained for the ex-situ RLS experiments. The resolidifed area contains elongated columnar like grains, with enormously enlarge width and length dimensions relative to the original 17 nm diameter grain of the Al film after sputter deposition (Figure 13). The elongated RLS grains originate at the edge of the melt pool, grew laterally, parallel to the temperature gradient and extend to the center. The elongated grains shown in Figure 13 are up to 5 μm long and about 0.5 μm wide. In this free-standing film without bulk substrate support the nucleation zone (Zone 4) reported in prior research on RLS processed Si bulk substrate supported metal films [2] does not develop.

Initially, two sets of free-standing aluminum thin films have been prepared, one set with and the other without a SiO_2 cap layer. The primary purpose of using the SiO_2 cap layer is to suppress possible de-wetting after melting and prior to solidification, since most liquid metal films on amorphous substrate de-wet upon complete melting [38]. In the pulsed-laser irradiation experiments of aluminum the native Al_2O_3 layer appears to assist with prevention of de-wetting for uncapped Al thin films. Hence, uncapped Al thin films were used for most experiments reported on here in order to minimize the background signal in TEM imaging and diffraction data caused by amorphous cap layers.

5.2.2 Microstructural Analyses

The ex-situ illuminated film was investigated to determine grain morphology, defect content and possible solidification zones. It is seen from the Figure 14a that the initially average grain size is

about 20 nm. At the position of the liquid-solid interface prior to the start of solidification a subset of grains widens dramatically to about 500 nm = 0.5µm at the expense of others which do not grow laterally. Thus, a small occlusion zone was observed. It should be noted here that unlike the conventional solidification processes, no nucleation is required in this experimental setup for RLS. The Al grains in the solid at the liquid-solid interface act as growth seeds that will simply grow when the temperature at the interface drops below the melting temperature. In the case of the free-standing film geometry there is no bulk Si substrate support that can act as a reservoir to absorb heat and the heat from the superheated melt is mainly transported through the liquid-solid interface and via the solid metal film. Hence, the melt pool will maintain a higher temperature than the solid and the solid-liquid interface. Therefore nucleation in the center, as is often observed in melting experiments of substrate supported films [e.g. 2], where the substrate acts as the mean heat sink, is not observed in the experiments for free-standing thin films presented here (Figure 14b).

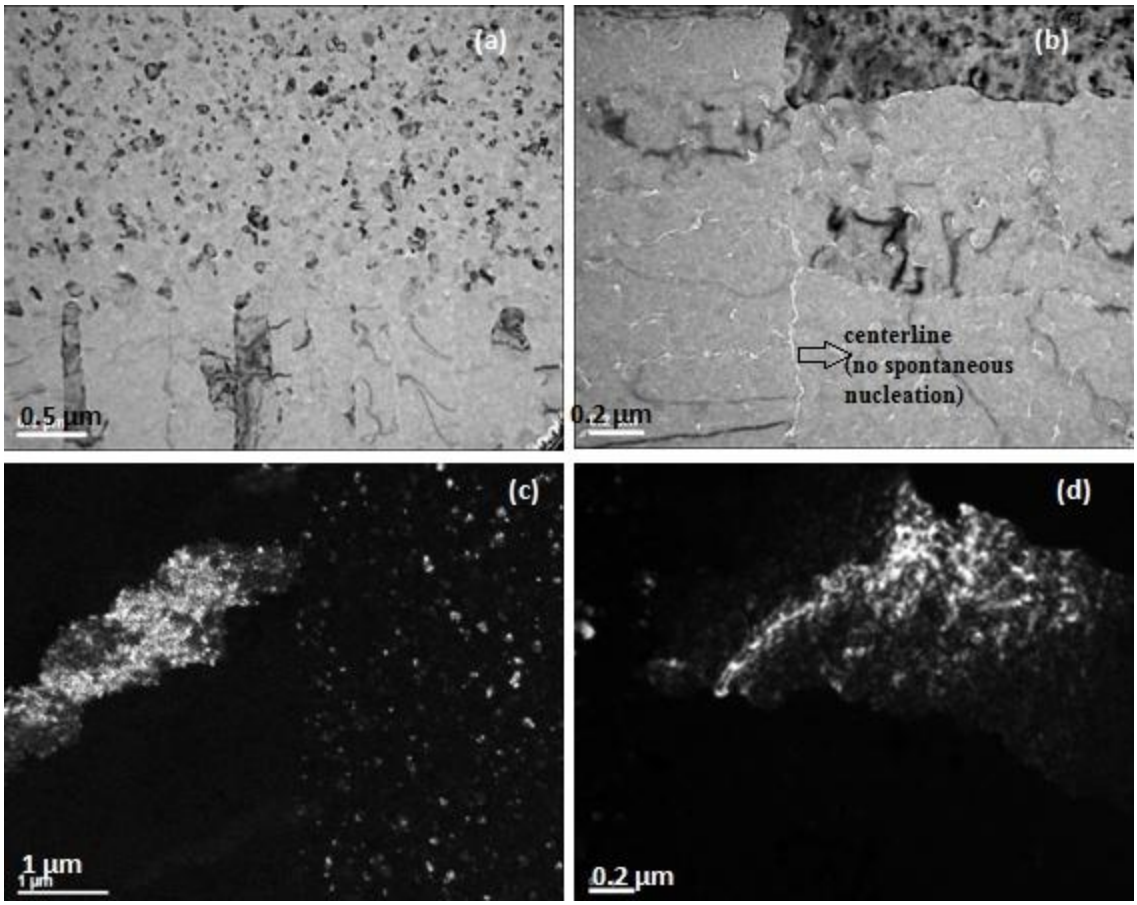

Figure 14. Ex-situ RLS microstructure a) bright field image of the illuminated boundary, b) bright field image of the center, c) dark field image of the grain boundary morphology, (d) dark field image of an elongated grain

Figure 14c and d show dark field images of an elongated grain. These images reveal that elongated grains exhibit rough grain boundary morphology and seem to be heavily defected in their interiors. It is seen from the Figure 14d that dislocation content in the grain interior seems to cause enough misorientation of the crystal lattice, i.e., change in deviation parameter, s, for the imaging condition to affect discernible variations in the diffraction contrast TEM images. Thus, different areas of a single grain to go in and out of Bragg condition and appear bright or dark. (Figure 14d.)

In the ex-situ experimentation a beam shape-limiting mask is used to control the dimensions of the illuminated sample area. Here we used a rectangular shaped mask, essentially a slit with variable width. An increase in slit width leads to a wider melt pool. Thereby longer elongated grains can be obtained. Eventually, if width becomes too large, radiation heat loses in the center of the melt pool is expected to becomes significant enough, so that nucleation and growth processes in the center of the melt pool might compete with the growth of the elongated columnar like grains. As a result, a nucleation and growth zone might be observable under these conditions. To date we have not performed such RLS grain length limiting experiments. In the future we plan to investigate how wide the melt pool can become before nucleation and growth processes occur to essentially terminate the RLS growth of the newly formed grains.

5.3 IN-SITU RLS MICROSTRUCTURE

5.3.1 Specimen Illumination

In-situ melting experiments of aluminum film were carried out by dynamic transmission electron microscopy (DTEM) (Figure 15a). A short and intense laser pulse from the hydro-drive laser is used to heat the specimen and induce a phase transformation (Figure 15b). A second synchronized time delayed laser pulse from the cathode drive laser is used to illuminate the photoelectron cathode, thereby creating an electron pulse, which then is used to either acquire an image or diffraction data (Figure 15b) [31-33]. Figure 15c shows in-situ illuminated area of the polycrystalline aluminum film.

The shape of illuminated are for in-situ melting is elliptical, quite different than that of ex-situ melting, the shape of the hydro-drive laser is round. As the hydro-drive laser illuminates the sample at a 45^{o} angle, the resulting shape of the melt pool becomes elliptical. Hence, re-solidified grain morphology could be expected to be dissimilar, especially towards the melt pool regions where the initial solid-liquid interface exhibit high curvatures. For the in-situ experiments study, the proper laser beam energy fluence to insure complete melting has been found to be in between 1.5 J/cm^2-3.8 J/cm^2.

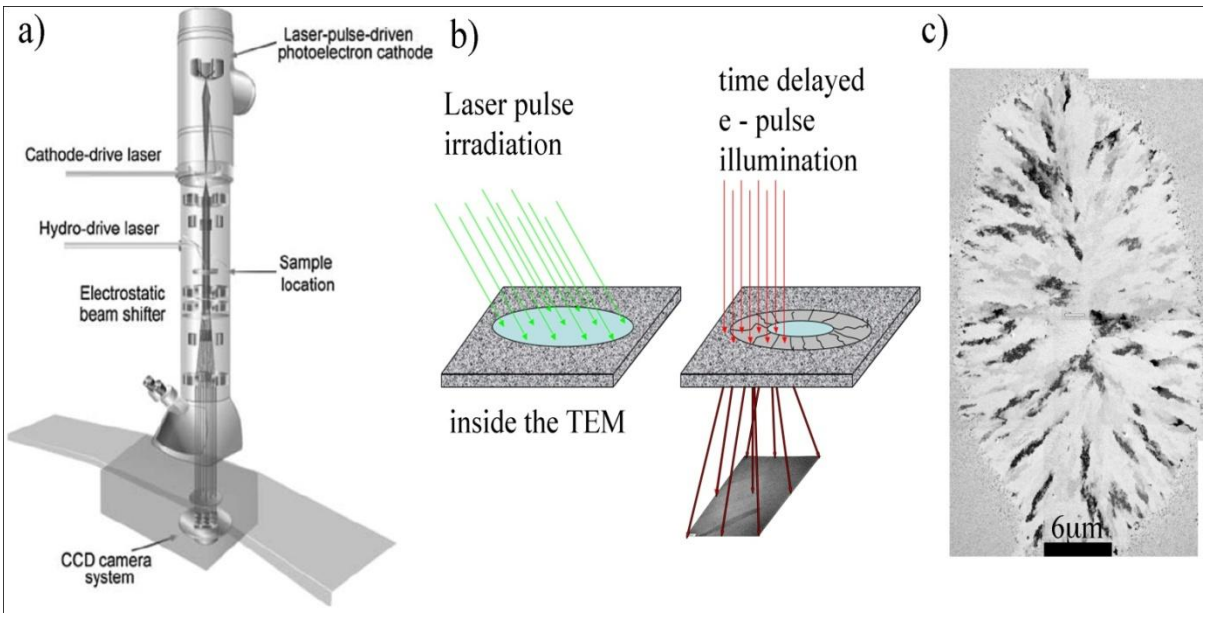

Figure 15. a) schematic of the DTEM, b) schematic of the experimental sequence, c) illuminated area and elongated grains

Figure 16 shows a serious of experiments taken after different time delays. As the microstructure is significantly modified after one laser shot, a new region was studied for each experiment using the same experimental conditions and the results were compared.

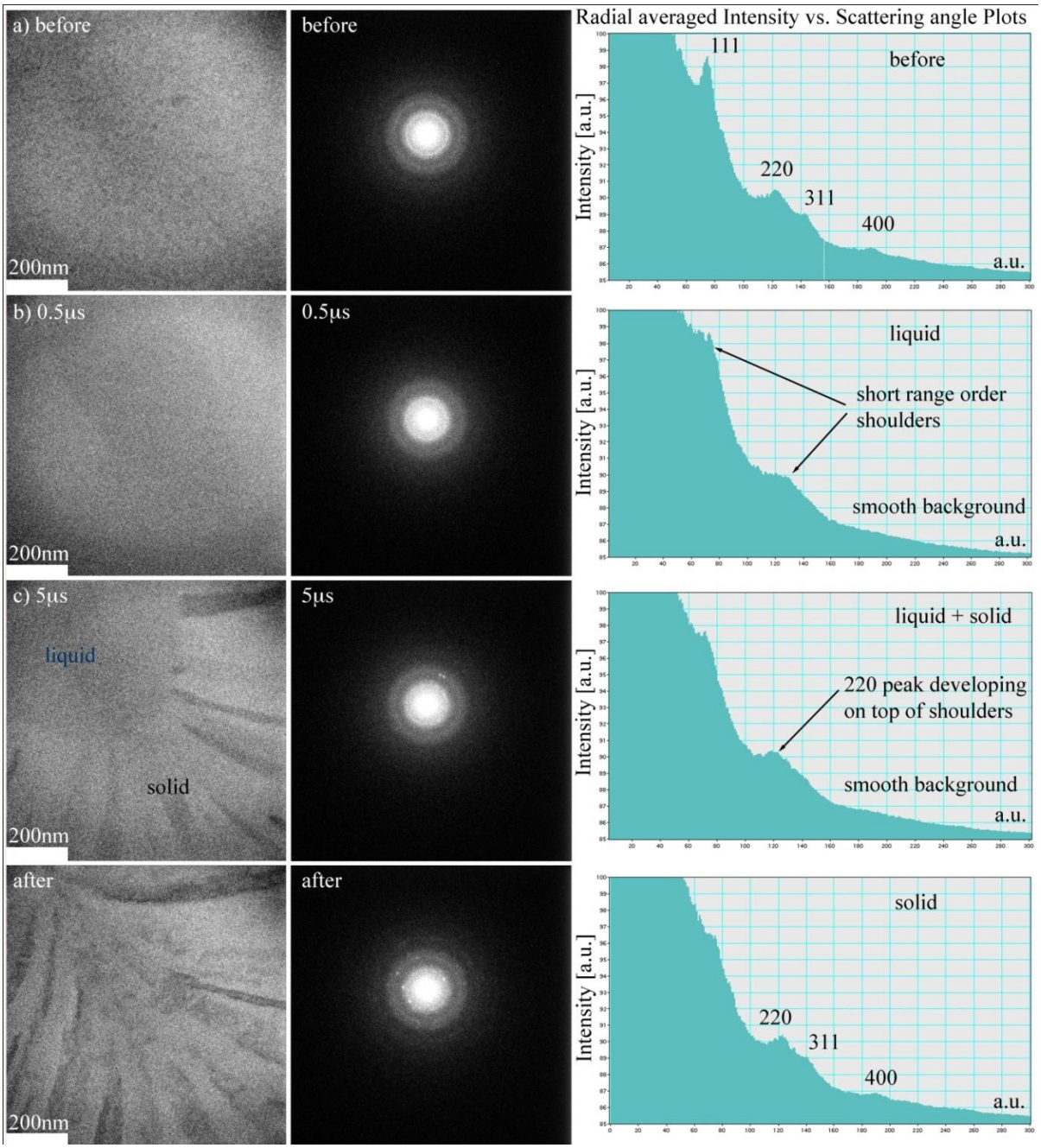

Figure 16. Images, diffraction patterns and radial average plots; (a) before melting, (b) at 0.5µs after the melting, (c) at 5 µs after the melting, (d) at long time after the melting

Figure 16 shows images, diffraction patterns and radially averaged plots of the to the diffraction patterns acquired before illumination (label 'before' in Fig. 16), during illumination (labels '0.5μs' and '5μs' in Fig. 16), and after complete solidification (label 'after' in Fig. 16). The image prior to the melting experiment shows little contrast variation because the magnification of 4000x used here is too low to resolve the nanocrystalline grains. The diffraction pattern and corresponding radial average plot taken before melting (Figure 16a) show diffraction rings and maxima characteristic of Al on top the amorphous signal of the Si_3N_4 membrane. After a delay time of 0.5 μs, the polycrystalline Al rings disappear and amorphous contrast is enhanced (Figure 16b). The Al film is liquid after melting it by pulsed laser irradiation at 0.5 μs prior. The signal of the amorphous liquid is added to the signal of the amorphous Si_3N_4 membrane in the diffraction pattern. After 5 μs of delay time, the solid-liquid interface moved into the field of view (Figure 16c). In the corresponding diffraction pattern clear distinct diffraction maxima in the form of 'spots' are observable. Distinct diffraction maxima develop on top of the amorphous signal in the corresponding radial average plot (Figure 16c). This implies that crystalline grains have formed and solidification is underway. After completion of solidification, the newly formed solid in the RLS processed region exhibits a diffraction pattern consistent with a polycrystalline Al film with enormously enlarged grain size relative to the as-deposited nanocrystalline thin film and much fewer different orientations are sampled in the field of view, resulting in a finite number of stronger diffraction spots (Figure 16d).

5.3.2 Solidification Interface

The image series displayed in Figure 17 show an image taken before illumination, during the solidification (t = 5 μs after the laser pulse for melting), and after completion of solidification.

Figure 17a shows polycrystalline aluminum film. Rapid conduction of heat into the unmelted region of the film initiates resolidification, i.e., the solid-liquid interface starts to move from the edge of the elliptically shaped melt-pool towards its center. As can be seen from the Figure 17b the solidification interface is planar as it is expected for a grain growth into superheated liquid in pure metals during solidification [10]. It should be noted that the resolution at this magnification (4000x) is limited. At higher magnifications disturbances might be observable. However, lateral resolution for the moving solidification front is also limited by the motion blur. In the very short by finite time of pulsed electron illumination for imaging, ~12ns, the moving solidification front travels a certain distance, Δx, which essentially represents the lateral resolution limit at any magnification of the TEM instrument during the DTEM experimentation. If the transformation front velocity were 10m/s than the motion blur limited lateral resolution for a 12ns imaging pulse, the effective exposure time, would be Δx=120nm. Since the effective exposure time is fixed to 12ns in the DTEM currently for different solidification front velocity different motion blur limited lateral resolutions result. Figure 17c was taken after completion of solidification, depicting long elongated grains extending from the melt pool edge towards its center.

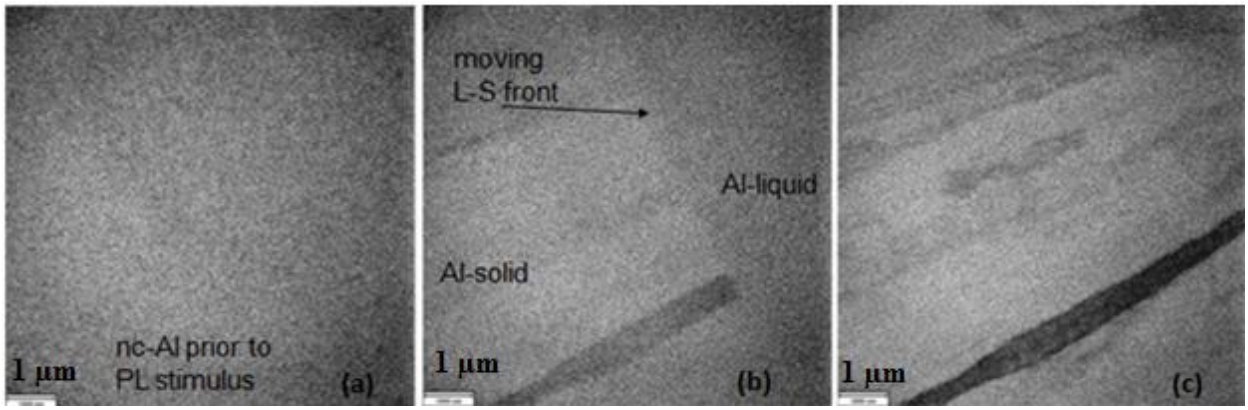

Figure 17. Images taken (a) before illumination, (b) at 5 µs after the melting, (c) after complete solidification

The DTEM experimentation also enables determination of the solid-liquid interface velocities, because it is possible to take images for different time delays to determine interface positions relative to the edge of the original melt pool after different time delays during the phase transformation. A serious of bright field TEM images of the solidification interface taken at different time delayes is shown in Figure 18. The interfacial velocities have been determined by measuring the changes in radius of the remaining melt pool with a change in time. It can be clearly seen from the figure that after 3.5 µs, the solid-liquid interface has not moved into the field of view yet. The illuminated region still consists entirely of liquid. The solid-liquid interface is in the field of view 4 µs after pulsed laser illumination. The velocity for this time frame has been determined to be ≈10 m/s. A deceleration to about 3-4 m/s happens fast, between 4.0-5.5 µs after illumination. The velocity then stabilizes as no further chance is observed until solidification is completed. In this set of single pulsed melting experiments, the solidification process is completed within 15 µs and a lower limit for the cooling rate has been estimated as $2*10^7$ K/s.

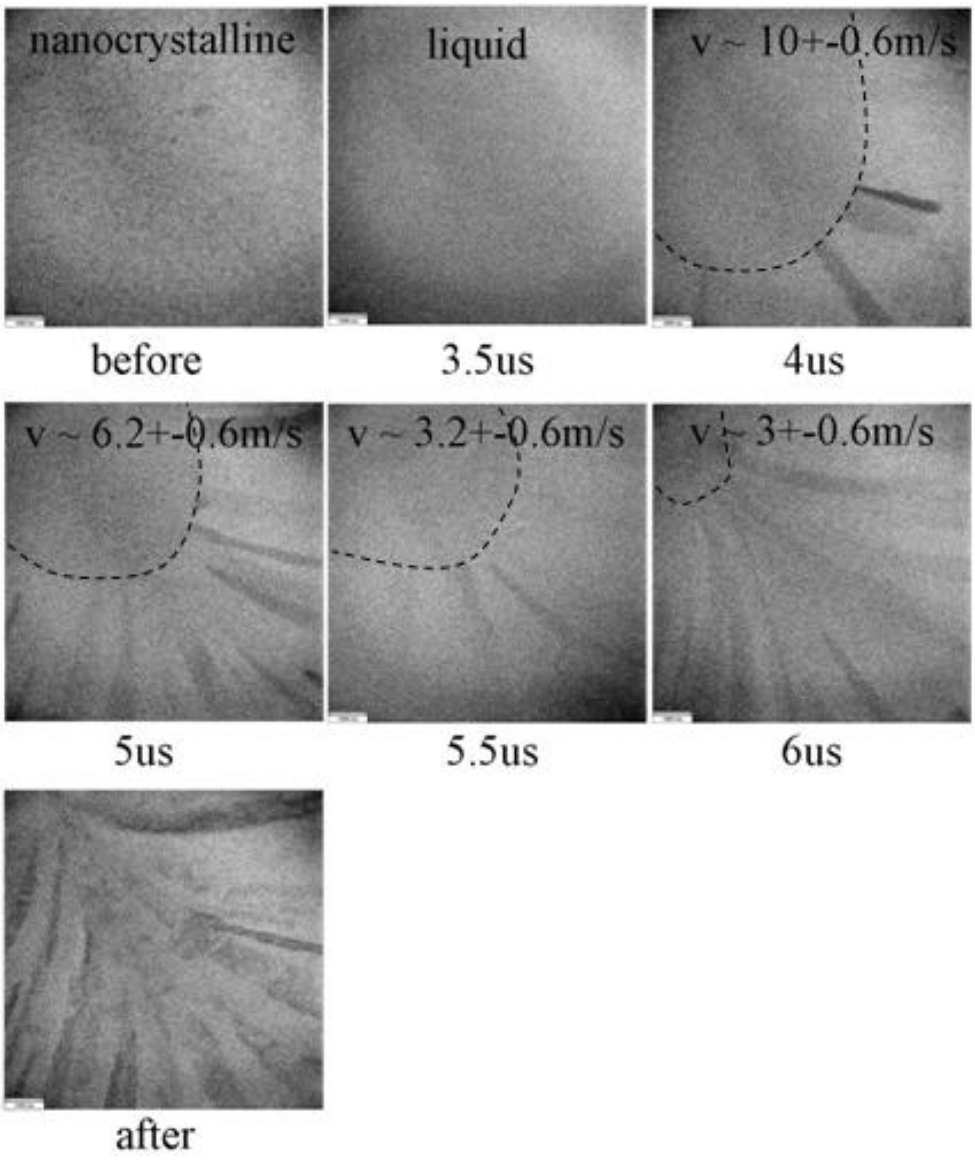

Figure 18. Serious of bright field images at different time delayed snapshots from different experiments

5.3.3 Grain Analysis

The in-situ RLS DTEM samples were used afterwards for detailed TEM analyses of the elongated grains that resulted in the elliptically shaped laser melted and RLS processed regions. Figure 19 shows bright field (BF) and dark field (DF) TEM images of an elongated grain and corresponding diffraction patterns. The images were taken from the newly formed grains at the boundary that solidification was initiated. They exhibit long elongated single crystalline grains formed from the sides of the unmelted regions toward the center of the melt pool. As can be seen from Figure 19 and 20 the elongated grains are up to 15 µm long and the widths of them are between 0.5 µm and 2 µm. Figure 20 also shows that the grain morphology is quite similar to that of ex-situ RLS processed Al thin films in the regions where the interface had small curvatures. Even in the high curvatures regions the grains are elongated, columnar. The growth of these grains follows the path of the highest temperature gradient.

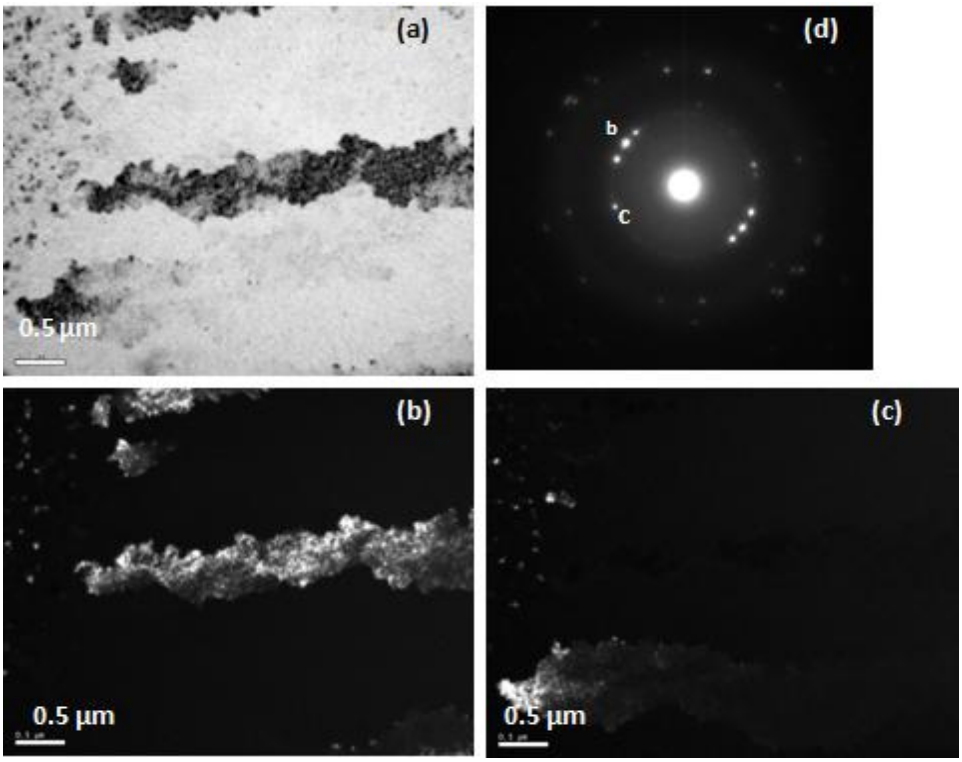

Figure 19. (a) Bright Field image, (b) and (c) Dark Field mages of elongated grain, (d) selected area diffraction pattern corresponding to dark field images

As can be seen from Figure 19b, the grain morphology with respect to roughness of the grain boundaries between the RLS grown grains after in-situ TEM melting experiments is quite similar to that after ex-situ melting experiments. Similarly, a narrow occlusion zone is observed after in-situ RLS of aluminum thin films. Initially small grains widen to over 0.5 µm width at the expense of other grains. Another image from the center of modified region was taken to investigate the possibility of competing nucleation towards the center of the melt pool (Figure 20) and no nucleation zone was observed. Grains that survived occlusion grow from the sides of the melt pool to the center and meet in the center without any interruptions caused by spontaneous nucleation and growth processes in the continuously cooling melt-pool ahead of the RLS front that grows from the edge of the original melt pool towards the center.

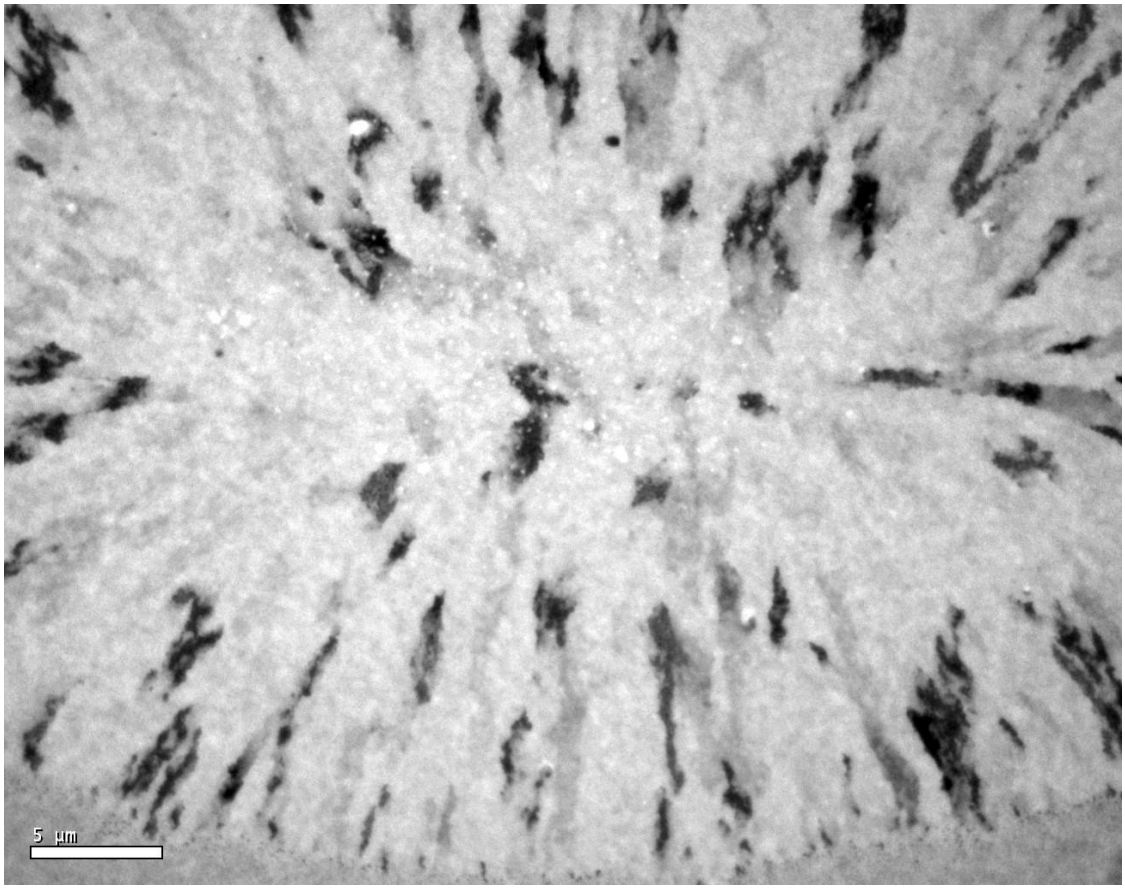

Figure 20. Bright Field image of in-situ illuminated region

During and after complete melting, heat flows into the unmelted region of the film, this heat flow warms up unmelted grains adjacent to melt pool and may cause grain growth. Hence, a heat affected zone (HAZ) may exist. We have examined the possible existence of a heat affected zone by quantitative microstructural analyses of the grain size and how it changes with distance from the original melt-pool edge. Dark field images of the nanocrystalline Al film have been collected at a suitable magnification in the TEM followed by analyses using the NIH Image image processing analysis program. Here regions that are 200nm wide have been used for binning the grain sizes representative of regions at different distances from the melt-pool edge.

An example of a TEM dark field image and the compiled summary of the grain size analysis conducted are shown in Figure 21.

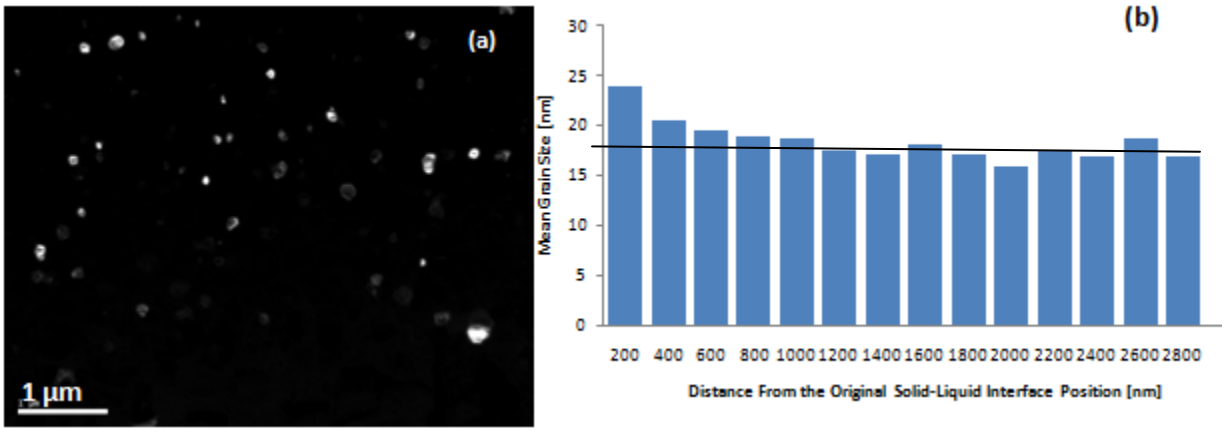

Figure 21. (a) Modified dark field image, (b) Corresponding mean grain size with respect to distance from the illuminated boundary

The average grain size in each 200 nm wide region at increasing distance from the melting pool boundary was calculated. Relative to the average grain size of 17 nm for the as-deposited thin Al film (solid line in Figure 21b) increases to an average grain size of 23.5nm and 20nm have been observed in the first and the second 200nm and wide regions directly adjacent to the melt-pool interface from which RLS commenced. So, only a very narrow heat affected zone, extending no farther than about 400nm into the solid from the original liquid-solid interface after pulsed laser melting was detected. In this narrow, ≈0.4 µm, region adjacent to the solid-liquid interface some grain growth, about 38% over the first 200nm and 18% over the next 200nm relative to the 17nm average of the as-deposited Al thin film, occurred, but then heat flow was apparently insufficient to cause sufficient temperature rise for further grain growth.

5.3.4 Defect Content

The elongated RLS grains have been investigated by TEM few days after in-situ DTEM melting experimentation and after a long time (8 weeks) of natural ageing or isothermal annealing at 300 K. Changes in defect concentration have been examined. Results are shown in Figure 22 and Figure 23.

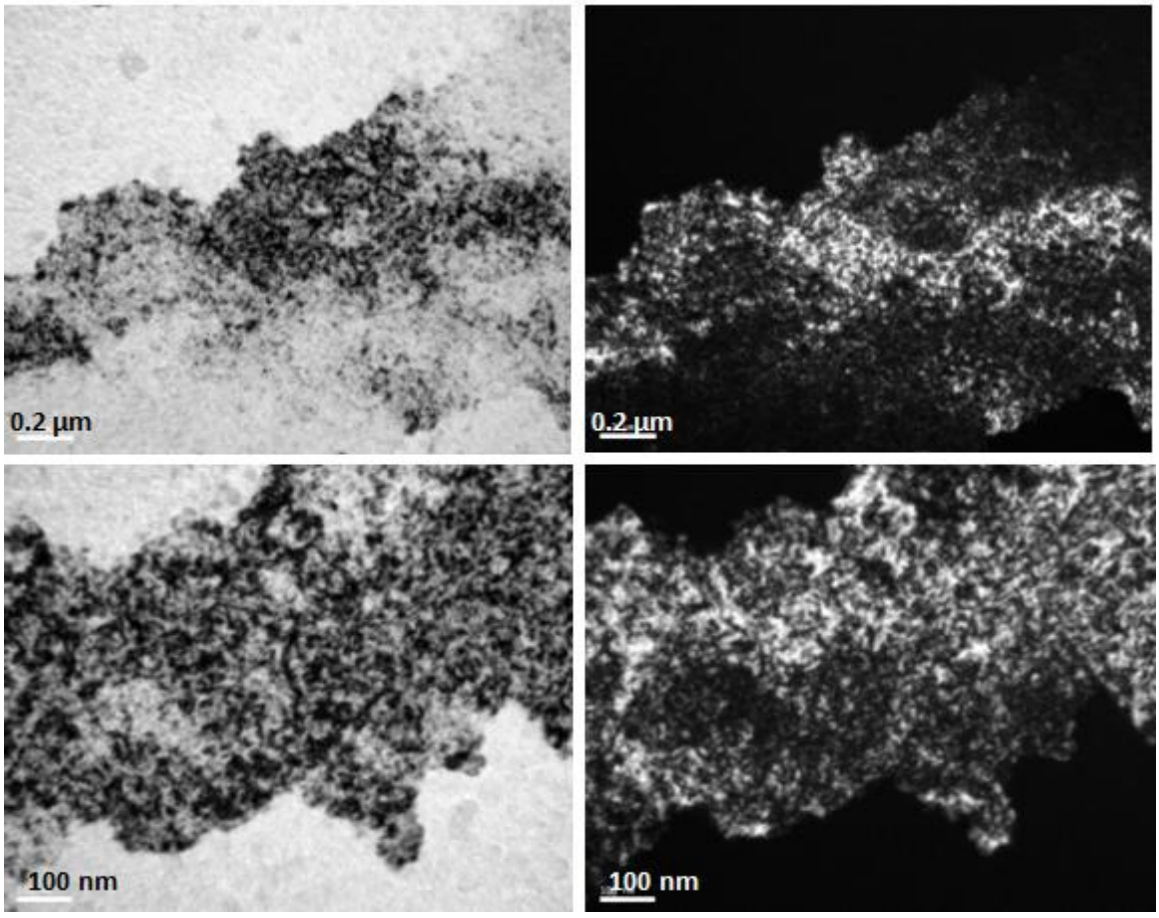

Figure 22. Bright field and dark field images at different magnifications after illumination of RLS grains in Al films after a few days of the RLS experiments

Figure 22 shows a series of bright field TEM images and dark field TEM images at various magnifications revealing a high concentration of defect content of the elongated grains after the melting and resolidification experiments. Tilting experiments and selected area diffraction pattern (not shown here) suggest that the elongated grains in Figure 22 are close to a diffraction condition and single crystalline. It was generally found that the elongated grains seem to be heavily defected after both the ex-situ RLS and the in-situ RLS experiments.

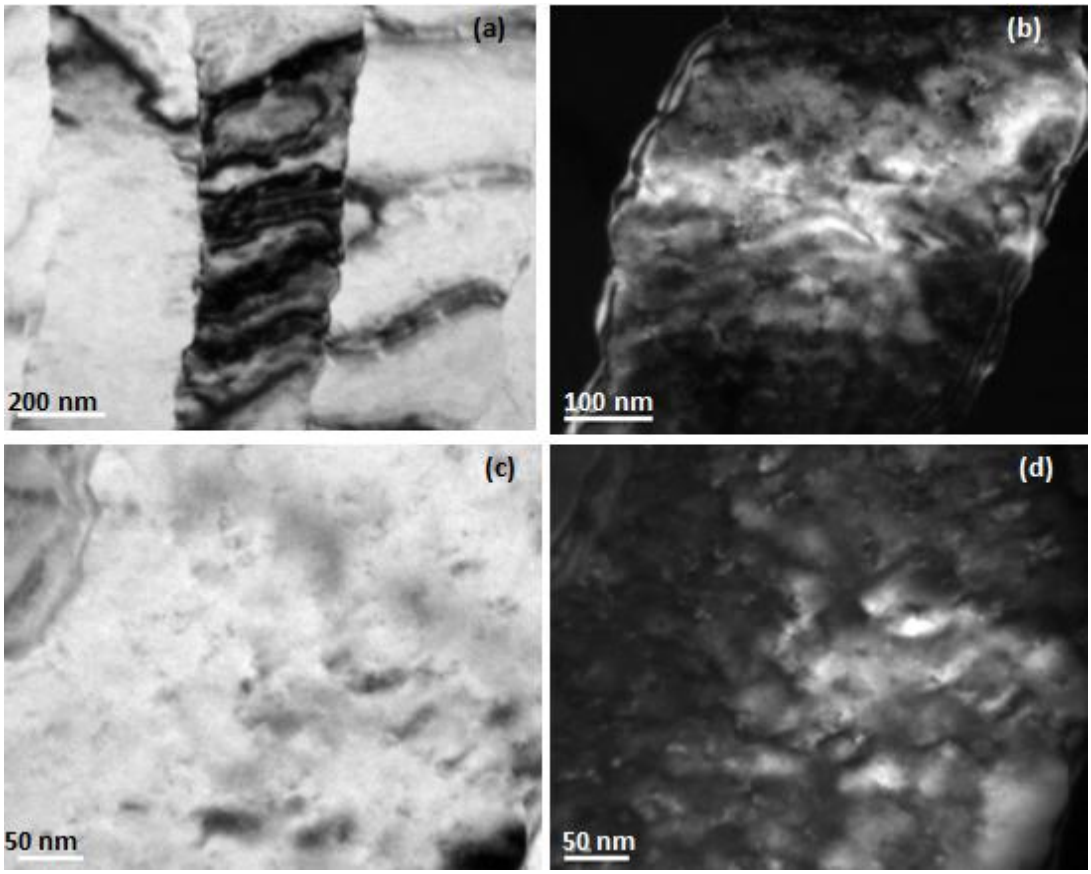

Figure 23. Dark field and Bright field images at various magnifications of elongated grains after 8 weeks additional time of 300 K annealing

After additional time (about 8 weeks) of 300 K annealing (equivalent to natural aging), additionally TEM analyses showed that high defect concentration of the elongated grains observed for shorter times (a few days) after the original RLS experiments now was vastly reduced and the morphologically rough grain boundaries appeared to have attained a much more straightened morphology (Figure 23). However, no newly formed grains are observable; suggesting that the resolidified Al thin films underwent recovery processes only but did not recrystallize.

6.0 DISCUSSION

6.1 GRAIN MORPHOLOGY

The 80nm thin Al films were heated above the melting point T_m (933 K for aluminum) by a single-pulsed-excimer laser irradiation. The current experiments indicate that pulse-laser-irradiation of aluminum thin film on amorphous substrate conducted under the conditions employed here does not lead to de-wetting upon complete melting prior to re-solidification. Speculatively, it can be proposed that the native grown Al_2O_3 oxide layer may be responsible for suppressing or slowing of the mechanisms associated with de-wetting. Upon complete melting, which is achieved if the pulse melts the entire film to the underlying amorphous Si_3N_4 membrane, solidification begins from the sidewalls of the melt pool and proceeds laterally toward the center. Importantly, under these geometrical, thermodynamic and kinetic solidification conditions no nucleation is required as Al grains at the solid-liquid interface will start to grow when the temperature drops below T_m. Hence, no undercooling, no nucleation event is required to initiate the solidification process. This transformation path is very similar to seeded solidification in which unmelted polycrystalline seeds assist the transformation. It should also be noted that the sidewalls composed of the unmelted polycrystalline seed material may not be sharply defined due to limitations of the excimer projection optics.

At the beginning of solidification grains quickly expand vertically through the thickness to span the full 80 nm film thickness. During growth the width of some grains increases at the expense of others, which are occluded. Occlusion is commonly observed in solidification of polycrystalline pure metals [2], which is typically attributed to the anisotropy in interfacial free energies [39].

Solidification regions extend about 15-20 μm for in-situ TEM melting and 4-5 μm for ex-situ melting, and consist entirely of elongated columnar grains, which seem to have grown parallel to the direction of the dominant thermal gradients, i.e., along the dominant heat flow direction. The width of the columnar grains observed here are about 0.5 μm for ex-situ melting and between 0.5-2.0 μm for in-situ melting.

TEM analyses of ex-and in–situ melting of aluminum thin film did not reveal spontaneous nucleation of new crystallites from the melt anywhere in the molten and re-solidified region. The reason is following. The microstructures produced by rapid lateral solidification (RLS) are unique in metal thin films and depend on thermal properties and geometry of the substrate. If the thermal conductivity of a substrate is poor or if the dimensions of the substrate layer are small, i.e., if the substrate is thin heat cannot be dissipated as fast as in thick substrates with good thermal conductivity. In the present work, a Si-TEM grid with a 100 nm thick membrane of amorphous silicon nitride, a-Si_3N_4, was used as support for the free-standing, electron-transparent Al thin films. As the support is only 100nm thick and the thermal conductivity of Si_3N_4 (30 W/mK) is about one order of magnitude smaller as compared to Al (237 W/mK), it can be concluded that heat flow through the substrate is negligible. Heat will

essentially be dissipated through the unmelted thin film parallel to the solidification direction. The temperature of the liquid will always be larger than T_m for the RLS experiments conducted here. Grain growth always occurs into the superheated liquid so there is no undercooling in the melt. Grains that survived occlusion grow from the sides of the melt pool to the center and meet in the center. As a result, a nucleation zone is not expected and consequently was not discerned in the pulse melting of aluminum thin films in this experimental geometry. In the case of thick substrates supporting the thin Al or metal film heat will be mainly transported through to the substrate. The temperature of the melt thus can drop below T_m, i.e., the liquid can become undercooled, and once a critical undercooling is reached nucleation and growth can become kinetically competitive to the lateral growth process from the sidewalls, in which case a nucleation zone will be observable [2].

6.2 SOLID-LIQUID INTERFACE

The dynamics of interface motion were observed in-situ by DTEM. The solid liquid interface velocity was determined measuring changes in interface position for known time intervals (Figure 18). The maximum velocity of the lateral solidification front was determined to be ~ 10 m/s at the onset of solidification and with progressing transformation the velocity decreases to an average velocity of ~ 3 m/s. (Figure 24).

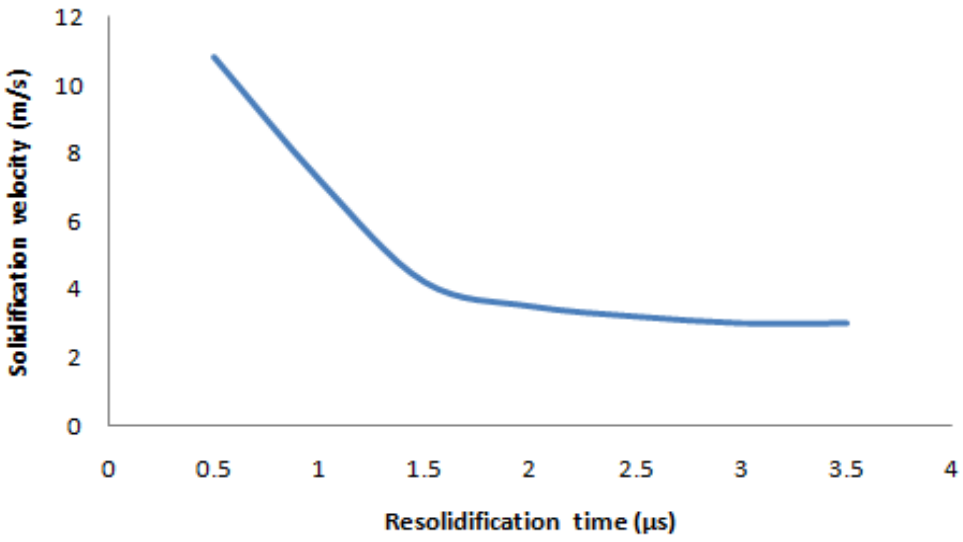

Figure 24. Solidification velocities as a function of resolidification time

At the beginning of the solidification heat flow into the unmelted grains is high as the surrounding unmelted film is cold and the resulting temperature gradient is highest. Hence, the interface velocity is also highest, v ~ 10 m/s. As the solidification continue, the surrounding film heats up, which leads to a decreased temperature gradient and a decrease in heat flow. As the film saturates with respect to thermal energy, i.e., heat, it can absorb and transport away from the liquid a steady-state transport rate is established with directly affects a steady state solidification

front velocity. The amount of heat that can be transported through the thin Al film away from the moving solidification interface will be limited by the heat that the thin film can transport away per unit time, which leads to a constant velocity of the liquid-solid interface. The deceleration of the interface to a stable velocity of ~ 3 m/s occurred between 4.0-5.5 μs after illumination and no further change was observed until solidification was completed. The steady-state RLS front velocity obtained in this work for the free-standing and uncapped Al thin film falls into the realm of RS conditions (solidification fronts moving faster than about 0.1m/s in metals [51]. However, RLS front speeds of 3m/s are about two orders of magnitude slower as compared to the velocities estimated from numerical computer models for the rapid lateral solidification front in RLS of encapsulated Cu thin film on bulk Si-substrate (v ~100-300 m/s) [2]. The rapid solidification geometry of Cu thin film is such, that the heat is mostly conducted away by the bulk substrate and also unmelted solids resulting in a much larger thermal gradient and concomitantly interfacial velocity.

In situ RLS experimentation showed that the liquid solid interface of Al thin films is planar during rapid lateral solidification. This is an expected result for solidification of a pure metal into a superheated liquid [40]. In pure metals, interface stability entirely depends on whether locally a perturbation can form that can conduct heat away faster than along the surrounding interface, i.e., whether a high temperature gradient can be maintained in the tip. As illustrated in Figure 25, in case of crystal growth into a superheated liquid, commonly when a perturbation forms at an initially smooth interface, the temperature gradient in the liquid increases while the gradient in the solid decreases. As the heat flux is proportional to the temperature gradient, more heat flows into the tip of the perturbation and less flows out of it into

the solid. As a result, the perturbation melts back and the planar interface is stabilized. It can be concluded that the solid-liquid interface of a pure metal, even at very high solidification rates, will always be stable if the temperature gradient is positive, as is seen in this study during rapid solidification of Al thin films.

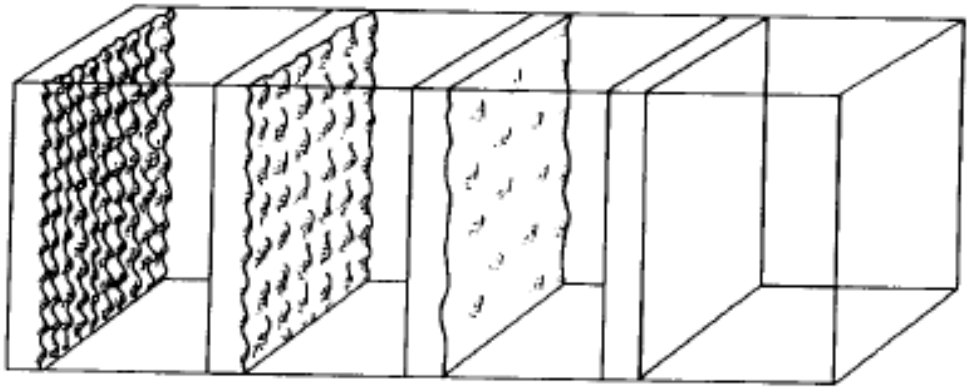

Figure 25. Initial evaluation of a stable interface [39]

6.3 DEFECT ANALYSES

Ex-situ and in-situ melting studies of Al thin film by a single-pulsed irradiation showed that elongated grains exhibit rough grain boundaries and grains are heavily defected after re-solidification. Defects can originate from two sources. Due to high quenching rates of at least ~$2*10^7$ K/s, non equilibrium high temperature vacancy concentrations can be quenched in during the cooling process in the re-solidified material, resulting in vacancies supersaturated Al thin film. Subsequently vacancies can cluster and form Frank loops on closed packed planes, thereby forming dislocations with Burgers vectors of the type 1/3<111>. Additionally, plastic deformation produced by quenching stresses due to differences in thermal expansion coefficients of the underlayer and the metal films could cause additional defect content, presumably in the form of glide dislocations with Burgers vectors of the type 1/2<110> [41].

Vacancies are equilibrium defects. At a finite temperature above absolute zero even in thermodynamic equilibrium there will be a finite defect concentration of vacancies in a crystal. The fractional concentration (C=n/N) of vacancies in a crystal as a function of temperature is given by [42, 43]

$$C = n/N = \exp(S_v/k).\exp(-h_v/kT)$$

where S_v and h_v are the vacancy formation entropy and enthalpy, respectively, n is the number of vacancies, N is the number of the lattice sites, k (= $8.617x10^{-5}$ eV/K) is the Boltzman constant and T the temperature. This equation can also be written as

$C = n/N = A. \exp -(Q/kT$

with A=8 and Q=0.76 eV for aluminum. Figure 26 also shows a schematic representation of vacancy concentration as a function of temperature. It can be seen that there is a sharp change in slope and a discontinuity in vacancy concentration at the melting point. The vacancy concentration of this plot was determined by rapid quenching of pure aluminum from different temperatures and lattice thermal expansions were measured.

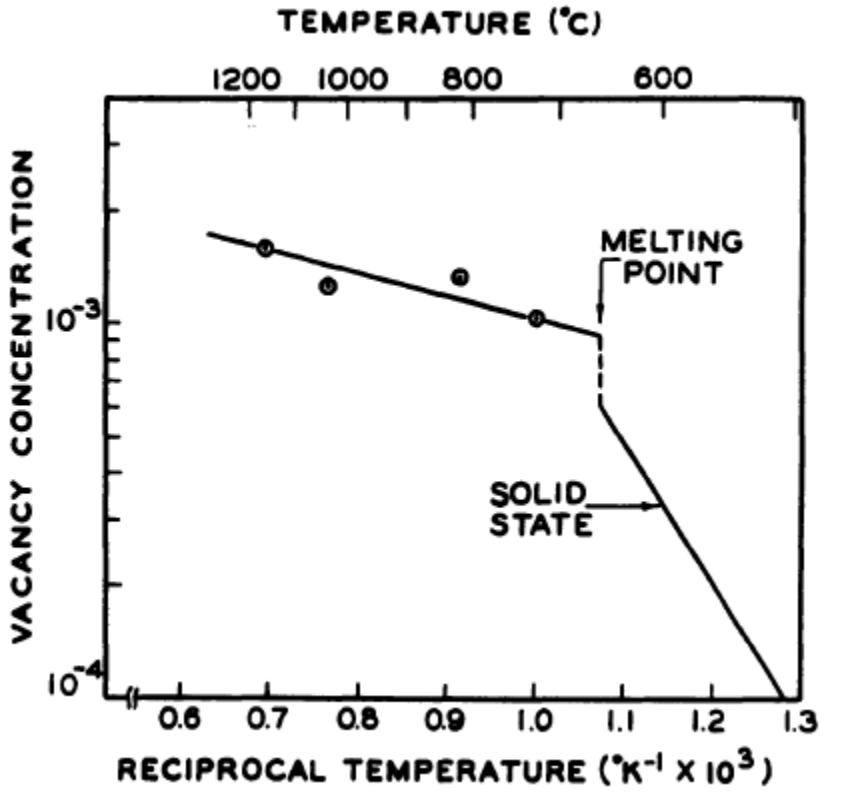

Figure 26. Relationship between vacancy concentration and temperature [42]

Due to the extremely high quenching rate ~ $2*10^7$ K/s during rapid solidification it is very likely that vacancy concentrations that commonly would only exist near the melting temperature are quenched in during rapid solidification of Al thin film. Many studies have been conducted to determine the vacancy concentration of pure aluminum near melting temperature

by different methods such as lattice thermal expansion measurement [43, 45, 46], electrical resistivity measurements [41], and transmission electron microscopy [42, 44]. They all presented similar vacancy concentrations of $9.4x10^{-4}$ – $1.3x10^{-3}$ or pure aluminum near melting temperature, which is 9 orders of magnitude higher as compared to the room temperature concentration of $1.3x10^{-12}$. Retention of such a high concentration of vacancies to lower temperatures, such a s 300K, will lead to the formation of vacancy disks, i.e., vacancy type Frank loops on closed packed planes, which could be consistent with some of the dislocation contrast observed during TEM analysis of the RLS processed Al thin film samples.

Another contribution to the high defect concentration in the columnar grains could stem from the difference between the thermal expansion coefficient of aluminum and silicon nitride, Si_3N_4. The thermal expansion of aluminum has been investigated by A. J. C Wilson [47] by measurement of the lattice spacing of Al as a function of temperature using a high temperature Deybe-Scherrer x-ray camera. The coefficient of expansion results are shown in Table 1. Thermal expansion coefficient of silicon nitride is $3x10^{-6}$ $C^{o\ -1}$ and does not change in a temperature range between room temperature and 1000 C^o [48].

Table 1. Thermal expansion coefficient of aluminum as a function of temperature

Temperature [C^o]	0	100	200	300	400	500	600	650
d [A]	4.0391	4.0486	4.0592	4.0701	4.0829	4.0947	4.1087	4.1162
10^6. α [$C^{o\ -1}$]	22	25.4	26.5	27.8	29.9	32.5	35.5	37.2

The thermal expansion of silicon nitride is much smaller than that of aluminum and it does not vary as rapidly with temperature as that of aluminum does. While the re-solidified aluminum thin film on silicon nitride substrate wants to contract as it cools down from the melting temperature to room temperature, it is being constrained by the Si_3N_4 substrate and therefore experiences eventually large tensile stresses. If these stresses exceed the yield stress of pure Al the Al thin film will plastically deform thereby increasing the defect concentration by production of glide dislocations, which could further contribute to the defect content in RLS grains and would also be consistent with the TEM observations. These dislocations would most likely be of the type 1/2 <110>.

After 8 weeks the RLS samples were investigated again by TEM. Bright and Dark field TEM images showed that the defect concentration was much lower and the grain boundaries less rough. However, no newly formed grains were observed, suggesting that the resolidified Al thin films underwent a recovery process rather than recrystallization. It is known that grain boundaries act as active vacancy sinks in quenched metals [44]. In thin film microstructure due to small grain size diffusion distance of the defects to grain boundaries is very short. In addition, as the melting point for pure Al is 933K, room temperature is still about ~ 1/3 of T_m, which is a significant fraction of the homologous temperature, vacancy facilitated reconfigurations of the defect structures may be possible. However, using the literature data for self-diffusion in Al with an equilibrium concentration of vacancies, it was calculated that an aluminum atom at room temperature moves on average only by about 3.3 Å over 8 weeks. Hence, in order to rationalize the observed rearrangement of atoms and reduction in defect content during the 8 weeks room temperature annealing, it is necessary to invoke a massively increased, non-equilibrium

concentration of vacancies. Given the very high quenching rates during the RLS experiments it appears reasonable to expect a large vacancy supersaturation in the RLS processed region of the Al films, which then could have assisted with annihilation and rearrangements of dislocations, including their relaxation into nearby dislocation sinks, i.e., grain boundaries. As grain boundaries relax and move through the crystal they also act as sinks for vacancies thereby additionally lowering the overall defect concentration, as observed by TEM.

7.0 SUMMARY AND CONCLUSIONS

Rapid lateral solidification (RLS) of polycrystalline microstructure 80 nm Al thin films on amorphous 100nm thick electron transparent Si_3N_4 support films has been studied. We successfully used single laser pulse irradiation to melt and induce rapid solidification in pure Al thin films both ex-situ in air and in-situ inside a TEM. Ex situ experiments were used to investigate the feasibility of rapid lateral solidification of Al thin films on amorphous substrate with and without cap layers and to use post mortem TEM to investigate the re-solidified microstructure. In situ experiments inside the DTEM at Lawrence Livermore National Laboratory were used to investigate the morphology of the moving solid liquid interface and the interfacial velocity.

The current experiments indicate that pulse-laser-irradiation of aluminum thin film on amorphous substrate does not lead to de-wetting upon complete melting and is possible without cap layer.

For the laser melted Al films analyzed here, solidification commenced at the edges of the molten line, and moves laterally toward the center of the melt pool. Heat flow is predominantly transported through the Al thin film. A small occlusion zone was observed at the position of the solid-liquid interface. Nucleation in the center was not observed for both ex-situ and in-situ

melting experiments. Re-solidified regions consist of single crystalline elongated columnar grains that extend from the edge of the melt pool to the center. Elongated columnar like grains have been found to be up to 15 µm and 5 µm long for in-situ and ex-situ melting, respectively.

Elongated grains obtained in-situ and ex-situ melting showed rough grain boundary morphology and seemed to be heavily defected after solidification. After annealing at 300 K, high defect concentration of elongated grains observed after the illumination was reduced and rough grain boundary observed after the illumination has been straightened.

The average solid-liquid interfacial velocity of about 3-4 m/s was determined by dynamic transmission electron microscopy. The initial velocity at the start of the re-solidification is ~ 10 m/s. The velocity decelerates over the next ~ 5.5 µs and stabilizes at ~ 3-4 m/s until solidification is completed. The liquid solid interface is planar, which is in good agreement with columnar growth into a superheated liquid.

After the successful investigation of rapid solidification of pure Al thin films we plan to explore the more complex phase front evolution that can occur in alloys thin films. In a first step we intend to study the effect of alloying elements on the stability of the solid liquid interface. We will try to investigate at which interfacial velocity the interfacial morphology changes from planar to dendritic. Furthermore, we will also increase the width of the irradiated region in order to investigate how large grains can be grown laterally.

BIBLIOGRAPHY

1. J.E. Kline and J.P. Leonard, Rapid lateral solidification of pure Cu and Au thin films encapsulated in SiO_2, Applied Physics Letters 86, 201902 (2005)

2. R. Zhong, A. Kulovits, J.M.K. Wiezorek, J.P. Leonard, Four-zone solidification microstructure formed by laser melting of copper thin films, Applied Surface Science 256, 105-111 (2009)

3. A. Kulovits, R. Zhong, J.M.K. Wiezorek, J.P. Leonard, Electron microscopy of geometrically confined copper thin films after rapid lateral solidification, Thin Solid Films 517, 3629-3634 (2009)

4. J.E. Kline and J.P. Leonard, Suppression of dewetting phenomena during excimer laser melting of thin metal films on SiO_2, Thin Solid Films 488, 306-313 (2005)

5. M. Hatano, S. Moon, M. Lee, K. Suzuki, C.P. Grigoropoulos, Excimer laser-induced temperature field in melting and resolidification of silicon thin films, Journal of Applied Physics, Volume 87, Number 1 (2000)

6. J.S. Im, H.J. Kim, M.O. Thompson, Phase transformation mechanisms involved in excimer laser crystallization of amorphous silicon films, Applied Physics Letters 63 (14) (1993)

7. S.R. Stiffler, M.O. Thompson, P.S. Peercy, Supercooling and nucleation of silicon after laser melting, Physical Review Letters, Volume 60, Number 24 (1988)

8. J. S. Im and H.J. Kim, On the super lateral growth phenomenon observed in excimer laser-induced crystallization of thin Si films, Applied Physics Letters 64 (17) (1994)

9. H. Saka, K. Sasaki, S. Tsukimoto, S. Arai, In-situ observation of solid-liquid interfaces by transmission electron microscopy, J. Mater. Res, Vol. 20, No. 7 (2005)

10. D.A. Porter, K.E. Easterling, Phase transformation in metals and alloys, p. 186-208 (1980)

11. R.E. Smallman and A.H.W. Ngan, Physical metallurgy and advanced materials, p. 37-45 (2007)

12. S.H. Davis, Theory of solidification, p. 7-42 (2001)

13. D.M. Herlach and P.K. Galenko, Rapid solidification; in-situ diagnostics and theoretical modeling, Materials Science and Engineering A 449-451, 34-41 (2007)

14. A. Prasad, H. Henein, E. Marie, A. Gandin, Understanding the rapid solidification of Al-4.3Cu and Al-17Cu using X-ray tomography, Metallurgical and Materials Transactions A, Volume 37A-249 (2006)

15. H. Jones, Review; The status of rapid solidification of alloys in research and application, Journal of Materials Science 19, 1043-1076 (1984)

16. B. Cantor, Microstructural development during rapid solidification, 22nd International Symposium on Materials Science, Denmark 2001

17. G.X. Wang, V. Prasad, Rapid solidification; Fundamentals and modeling, Annual Review of Heat Transfer, Issue 11, p. 207-305 (2000)

18. T.R. Anantharaman and C. Suryanarayana, Rapidly solidified metals, p. 1-19 (1987)

19. A.O. Olofinjana and A. Atrens, Properties of rapidly solidified binary copper alloys, Materials Letters 31, 87-92 (1997)

20. K. Fisher, Fundamental of solidification, p. 21-35 (1998)

21. N.H. Pryds and J.H. Hattel, Numerical modeling of rapid solidification, Modeling Simul. Mater. Sci. Eng. 5, 451-472 (1997)

22. K. Fisher, Fundamental of solidification, p. 45-63 (1998)

23. H.J. Kim and J.S. Im, New excimer laser crystallization method for producing large grained and grain boundary location controlled Si films for thin film transistors, Appl. Phys. Lett. 68 (11) (1996)

24. J. B. Choi, Pulsed laser induced melting and solidification of Al thin films, PhD Thesis, Columbia University (2006)

25. L. Mariucci, A. Pecora, R. Carluccio, G. Fortunato, Advanced excimer laser crystallization techniques, Thin Solid Films 383, 39-44 (2001)

26. M. Ohring, Materials science of thin films, p. 203-224 (2002)

27. A. Kulovits, J. Leonard, J. Wiezorek, Influence of processing parameters on microstructure of pulsed laser deposited Au thin films, Materials Research Society, Vol. 979, p. 91-96 (2007)

28. J.A. Thornton, Influence of apparatus geometry and deposition conditions on the structure and topography of thick sputtered coatings J. Vac. Sci. Tech. Vol. 11, Issue. 4, 666-670 (1974)

29. J.E. Kline, Suppression of dewetting in pulsed laser melting of thin metallic films on silica, MS Thesis, University of Pittsburgh (2005)

30. G.X. Wang, V. Prasad, Microscale heat and mass transfer and non-equilibrium phase change in rapid solidification, Materials Science and Engineering A292, 142-148 (2000)

31. W. W. King, M. Armstrong, V. Malka, B.W. Reed, A. Rousse, Ultrafast imaging of materials; exploring the gap of space and time, MRS Bulletin, Volume 31, 614-619 (2006)

32. J.M. Howe and H. Saka, In-situ transmission electron microscopy studies of the solid-liquid interface, MRS Bulletin, 951-957 (2004)

33. J. Boneberg, J. Bischof, P. Leiderer, Nanosecond time-resolved reflectivity determination of the melting of metals upon laser annealing, Optic Communication 174, 145-149 (2000)

34. T. LaGrange, G.H. Campbell, J.D. Colvin, B. Reed, W.E. King, Nanosecond time resolved electron diffraction studies of the α-β in pure Ti thin films using the dynamic transmission electron microscope (DTEM), J. Mater. Sci. 41, 4440-4444 (2006)

35. T. Lagrange, M.R. Armstrong, K. Boyden, C.G. Brown, G.H. Campbell, J.D. Colvin, W.J. DeHope, A.M. Frank, D.J. Gibson, F.V. Hartemann, J.S. Kim, W.E. King, B.J. Pyke, B.W. Reed, M.D. Shirk, R.M. Shuttlesworth, B.C. Stuart, B.R. Torralva, Single

shot dynamic transmission electron microscopy, Applied Physics Letters 89, 044105 (2006)

36. S.T. Picraux and L.E. Pope, Tailored surface modification by ion implantation and laser melting, Science, Volume 226, Number 4675 (1984)

37. B. Basu, Critical heat transfer analysis of pulsed laser melting of pure metals, Appl. Phys. Lett. 58 (6) (1991)

38. J. Bischof, D. Scherer, S. Herminghaus, P. Leiderer, Dewetting models of thin metallic films; nucleation of holes and spinodal dewetting, Physical Review Letters, Volume 77, Number 8 (1996)

39. D.Y. Li, J.A. Szpunar, A possible role for surface packing density in the formation of {111} texture in solidified FCC metals, J. Mater. Sci. Lett. 13, 1521 (1994)

40. K. Fisher, Fundamental of solidification, p. 45-85 (1998)

41. P.K. Rastogi, K. Mukherjee, Defects in liquid quenched from the liquid state, Metallurgical Transactions, Vol. 1, 2115-2117 (1969)

42. G. Thomas, R.H. Willens, Defects in aluminum quenched from the liquid state, California Institute of Technology (1963)

43. B.S. Nenno, J.W. Kauffman, Detection and determination of equilibrium vacancy concentration in aluminum, Journal of the physical society of Japan, Vol. 15, No. 2 (1960)

44. J.A. McComb, S. Nenno, M. Meshii, Structure of liquid-quenched aluminum, Journal of the physical society of Japan, Vol. 19, No. 9 (1964)

45. B.V. Guerard, H. Peisl, R. Zitzmann, Equilibrium vacancy concentration measurements on aluminum, Appl. Phys. 3, 37-43 (1974)

46. R.O. Simmons, R.W. Balluffi, Measurements of equilibrium vacancy concentration in aluminum, Physical Review, Vol. 117, No. 1 (1960)

47. A.J.C. Wilson, The thermal expansion of aluminum from 0º to 650 ºC, Phys. Soc. LIII, 3 (1940)

48. R. Minikayev, W. Paszkowicz, P. Piszora, M. Knapp, C. Bahtz, Thermal expansion of α and β silicon nitride

49. W. DeSorbo, D. Turnbull, Kinetics of vacancy motion in high purity aluminum, Physical Review, Vol. 115, No. 3 (1959)

50. S. Shingubara, Y. Nakasaki, Electromigration in a single crystalline submicron width aluminum interconnection, Appl. Phys. Lett. Volume: 58 (1) (1991)

51. K. Fisher, Fundamental of solidification, p. 133-153 (1998)